

Anilinoquinazoline Inhibitors of Fructose 1,6-Bisphosphatase Bind at a Novel Allosteric Site: Synthesis, In Vitro Characterization, and X-ray Crystallography

Stephen W. Wright,^{*,†} Anthony A. Carlo,[†] Maynard D. Carty,[†] Dennis E. Danley,[†] David L. Hageman,[†] George A. Karam,[†] Carolyn B. Levy,[†] Mahmoud N. Mansour,[†] Alan M. Mathiowetz,[†] Lester D. McClure,[†] Nestor B. Nestor,[†] R. Kirk McPherson,[†] Jayvardhan Pandit,[†] Leslie R. Pustilnik,[†] Gayle K. Schulte,[†] Walter C. Soeller,[†] Judith L. Treadway,[†] Ing-Kae Wang,[†] and Paul H. Bauer[‡]

Pfizer Central Research, Eastern Point Road, Groton, Connecticut 06340, and Pfizer Discovery Technology Center, 620 Memorial Drive, Cambridge, Massachusetts 02139

Received October 24, 2001

The synthesis and in vitro structure–activity relationships (SAR) of a novel series of anilinoquinazolines as allosteric inhibitors of fructose-1,6-bisphosphatase (F16BPase) are reported. The compounds have a different SAR as inhibitors of F16BPase than anilinoquinazolines previously reported. Selective inhibition of F16BPase can be attained through the addition of appropriate polar functional groups at the quinazoline 2-position, thus separating the F16BPase inhibitory activity from the epidermal growth factor receptor tyrosine kinase inhibitory activity previously observed with similar structures. The compounds have been found to bind at a symmetry-repeated novel allosteric site at the subunit interface of the enzyme. Inhibition is brought about by binding to a loop comprised of residues 52–72, preventing the necessary participation of these residues in the assembly of the catalytic site. Mutagenesis studies have identified the key amino acid residues in the loop that are required for inhibitor recognition and binding.

Introduction

Diabetes is one of the most prevalent diseases worldwide, and the incidence of this disease continues to grow. Noninsulin-dependent, or type 2, diabetes accounts for 90% of all diabetics and is estimated to affect about 6% of the population in the U.S. Hallmarks of the disease include fasting hyperglycemia and exaggerated postprandial glucose levels. Complications of type 2 diabetes include retinopathy, nephropathy, neuropathy, and coronary heart disease and are believed to be triggered by excessive protein glycation, which in turn results from excessive levels of circulating glucose. Clinical studies have been carried out to define the primary defect that causes the elevated fasting blood glucose levels observed in type 2 diabetics. The results have suggested that excessive hepatic glucose output is a principal cause.¹ Hepatic glucose output, in turn, derives from the breakdown of hepatic glycogen (glycogenolysis) and synthesis of glucose from 3-carbon fragments such as pyruvate (gluconeogenesis). Gluconeogenic flux has been shown to be excessive in type 2 diabetics.² Gluconeogenesis is a highly regulated and well-understood pathway. Fructose-1,6-bisphosphatase (F16BPase) is an enzyme expressed predominantly in the liver and kidney and is one of the rate-limiting enzymes of hepatic gluconeogenesis. In diabetes, the lack (type 1) or resistance (type 2) to insulin alters the gene expression pattern in the liver, such that all three of the rate-controlling enzymes of gluconeogenesis (PEPCK, F16BPase, and G6Pase) are upregulated.³ Diabetes coordinately upregulates these gluconeogenic

enzymes, while at the same time downregulating the opposing glycolytic enzyme gene expression. Hence, the substrate cycles are reset to increase net glucose production (gluconeogenesis) at the expense of glucose utilization (glycolysis) or storage (glycogenesis). Liver F16BPase activity has been shown to be elevated in insulin-deficient and insulin-resistant animal models of diabetes, highlighting the importance of this enzyme in the control of blood glucose.⁴

The physiologically relevant form of F16BPase is a homotetramer⁵ and exists in distinct conformational states (T and R), depending on the relative concentrations of active site and allosteric site ligands. The enzyme is subject to competitive substrate inhibition by fructose-2,6-bisphosphate⁶ and to allosteric inhibition by adenosine 5'-monophosphate (AMP).⁷ Fructose-2,6-bisphosphate and AMP synergistically stabilize the T state conformation, which is an inactive form of the enzyme, while the substrate fructose-1,6-bisphosphate stabilizes the kinetically active R state conformer. The regulation and molecular basis of F16BPase enzyme activity have been deduced from crystallographic studies utilizing the recombinant human fructose-1,6-bisphosphatase protein.⁸ A F16BPase inhibitor should reduce hepatic glucose output and lower blood glucose by inhibiting the elevated rate of gluconeogenesis present in diabetic patients and would thus represent a useful therapy for the treatment of type 2 diabetes. To this end, the naturally occurring AMP analogue ZMP (AICARiboside monophosphate)⁹ as well as a number of synthetic purine and other heterocyclic phosphonic acids have been described as potential antidiabetic agents,¹⁰ as have a series of piperazinediones.¹¹

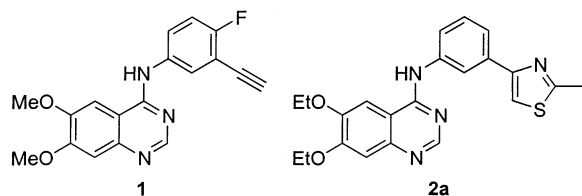
We recently reported our discovery that a series of anilinoquinazolines such as **1**, previously described as

* To whom correspondence should be addressed. Tel: 860-441-5831. Fax: 860-715-4483. E-mail: stephen_w_wright@groton.pfizer.com.

[†] Pfizer Central Research.

[‡] Pfizer Discovery Technology Center.

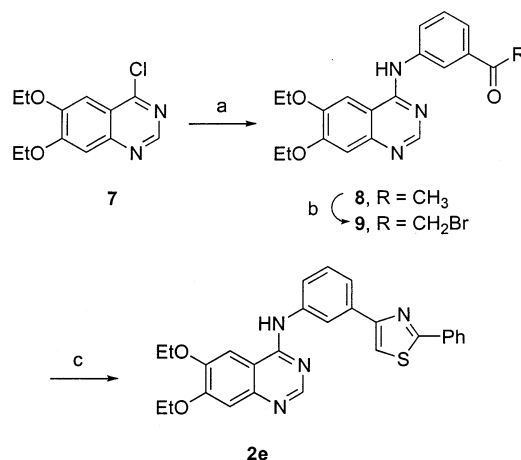
competitive inhibitors at the adenosine 5'-triphosphate (ATP) site of epidermal growth factor receptor tyrosine kinase (EGFR), were allosteric inhibitors of F16BPase ($IC_{50} = 0.25 \mu\text{M}$).¹² These compounds were identified by screening a library of compounds, known to be enzyme inhibitors that compete with AMP and/or ATP, against purified recombinant human F16BPase.¹³ Anilinoquinazolines **1** represent the first low molecular weight (<500) inhibitors of F16BPase that are not fructose or purine phosphates or phosphonates. We pursued this series as a template for further drug design, seeking to identify compounds that were structurally novel and selective for F16BPase inhibition, devoid of tyrosine kinase inhibitory activity. During the course of this work, we identified the thiazole-substituted anilinoquinazoline **2a** as a F16BPase inhibitor ($IC_{50} = 0.64 \mu\text{M}$) that was structurally novel and considerably less potent as an EGFR tyrosine kinase inhibitor (EGFR $IC_{50} = 4.8 \mu\text{M}$) than the halogen- and alkyne-substituted anilinoquinazolines such as **1** (EGFR $IC_{50} = 4 \text{ nM}$). In this paper, we describe studies of the F16BPase inhibitory activity of heterocycle-substituted anilinoquinazolines. The synthesis, *in vitro* biological activity, and mode of binding of these compounds are described, and the structure-activity relationships (SAR) are discussed with respect to five key structural features of these compounds: (i) the substituent on the thiazole ring (A); (ii) the thiazole ring itself (B); (iii) substituents on the isolated phenyl ring (C); (iv) the quinazoline 2-substituent (D); and (v) the quinazoline benzo-ring substituents (E). The mode of binding of these compounds to a novel allosteric site at the subunit interface of the F16BPase homotetramer was identified by X-ray crystallography. The amino acid residues that are most critical for binding to this novel site were subsequently determined by site-directed mutagenesis experiments.



Synthesis

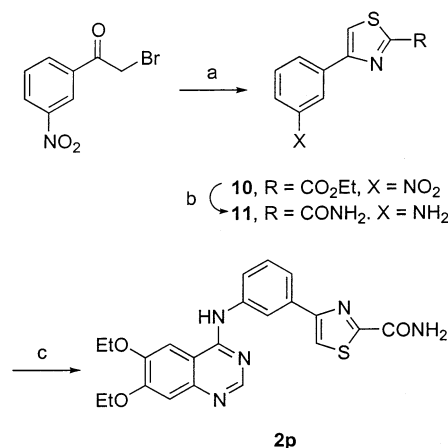
The thiazole-substituted anilinoquinazolines were prepared by any one of five different routes, to permit the efficient systematic variation of the various structural features of the molecule. The first route (Scheme 1) was designed to permit rapid variation of the thiazole ring substituent T_2 . 4-Chloro-6,7-diethoxyquinazoline (**7**, see Experimental Section for preparation from 3,4-diethoxybenzoic acid) was converted to the phenacyl bromide **9**, which was then condensed with a commercially available thioamide ($T_2\text{CSNH}_2$). Certain thiazole ring substituents, for example, CH_2OH (**2g**) and CONH_2 (**2p**), for which the precursor thioamides were unavailable, were prepared by functional group manipulation prior to formation of the penultimate anilinoquinazoline. In these cases (Scheme 2), the reaction of 3-nitrophenacyl bromide with a substituted thiourea was followed by the necessary functional group manipulation and ultimately by reduction of the nitro group.

Scheme 1^a



^a Reagents: (a) 3-Aminoacetophenone, EtOH, reflux. (b) Br_2 , HBr, AcOH, reflux. (c) PhCSNH₂, EtOH, reflux.

Scheme 2^a



^a Reagents: Ethyl thiooxamate, EtOH, reflux. (b) (i) SnCl_2 , HCl, EtOH, reflux; (ii) NH_3 , EtOH, 20 °C. (c) Compound **7**, EtOH, reflux.

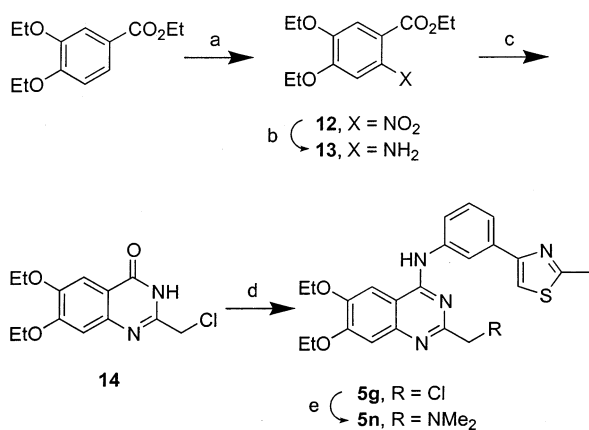
Condensation of the resulting aniline with **7** afforded the desired target.

Replacement of the thiazole ring by other heterocyclic rings or carbocyclic aromatic rings was accomplished by a palladium-catalyzed Suzuki coupling of the appropriately substituted aryl bromide with 3-nitrophenylboronic acid, followed by reduction of the nitro group and condensation of the resulting aniline with **7**.

Replacement of the 4-phenylthiazole ring by the 2-phenylthiazole regioisomer was accomplished by treating 3-nitrothiobenzamide with the appropriate α -halocarbonyl compound followed by reduction of the nitro group and condensation of the resulting aniline with **7**.

The synthesis of thiazole-containing analogues bearing additional substituents on the isolated phenyl ring proceeded via a Hantzsch thiazole synthesis with thioacetamide and the substituted 3-nitrophenacyl bromide, followed by reduction of the nitro group and condensation of the resulting aniline with **7**.

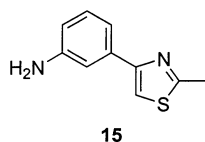
Variation of the quinazoline substituents at the 2-position or on the quinazoline benzo ring required preliminary construction of the appropriate 2-substituted quinazolin-4-one. Substituents at the quinazoline 2-position were introduced by the reaction of 2-amino-4,5-diethoxybenzoic acid ethyl ester (**20**) with a nitrile

Scheme 3^a

^a Reagents: HNO₃, AcOH, 20 °C. (b) H₂, Pd–C, EtOH, 20 °C. (c) ClCH₂CN, HCl, 20 °C. (d) (i) POCl₃, reflux; (ii) Compound **15**, 2-PrOH, reflux. (e) Me₂NH, 1,4-dioxane, 80 °C.

Q₂CN in the presence of hydrogen chloride to afford the quinazolin-4-one, followed by conversion to the 2-substituted-4-chloroquinazoline with phosphorus oxychloride (Scheme 3).

Substituents on the benzo ring of the quinazoline were generally attached via ether linkages. When the desired dialkoxy substitution pattern was commercially available, the appropriate anthranilate ester was heated with either neat formamide or formamidinium acetate in ethanol to afford the quinazolin-4-one. Other anthranilate ester starting materials were prepared by alkylation of a hydroxybenzaldehyde derivative, followed by oxidation of the aldehyde to the acid with potassium permanganate, Fischer esterification, nitration, and reduction of the nitro group. The quinazolin-4-one was then transformed to the 4-chloroquinazoline with phosphorus oxychloride. The 4-chloroquinazolines thus obtained were subsequently condensed with the desired (3-amino)phenylthiazoles, usually 3-(2-methyl-thiazol-4-yl)-phenylamine (**15**).



In most cases, the target anilinoquinazolines precipitated from the reaction mixtures in which they were prepared in analytically pure form and were isolated by filtration and washing with additional solvent followed by drying. Some products precipitated as HCl or HBr salts, while in other cases the products precipitated without the formation of an acid addition salt.

Evaluation of Enzyme Inhibition

Recombinant human F16BPase activity was assayed by measuring the inorganic phosphate hydrolyzed from fructose-1,6-bisphosphate by the enzyme. The phosphate released was quantified spectrophotometrically as a complex with ammonium molybdate and malachite green.¹⁴ The assay was run under saturating concentrations of substrate (500 μM) due to the low *K_m* of F16BPase for its substrate and the sensitivity of the phosphate detection method. Under these conditions, the assay was linear with time and enzyme concentra-

Table 1. Variation of the Thiazole 2-Position Substituent

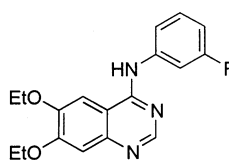
compd	T ₂	mp (°C)	F16BP (IC ₅₀ , μM) ^a	EGFR (IC ₅₀ , μM) ^b
2a	Me	259–260	0.64	4.8 (86%)
2b	H	265–266	0.39	0.018
2c	<i>c</i> -C ₃ H ₅	227–229	0.83	(90%)
2d	<i>n</i> -C ₃ H ₇	229–232	> 10	n.d. ^c
2e	Ph	274–275	> 10	n.d.
2f	CH ₂ Ph	265–266	> 10	n.d.
2g	CH ₂ OH	251–252	0.83	(96%)
2h	CH ₂ OMe	232–233	7.3	n.d.
2i	NH ₂	256–259	3.5	0.56
2j	NHMe	252–253	0.80	(74%)
2k	NMe ₂	195–198	8.0	n.d.
2l	N ₂ H ₃	239–242	4.5	n.d.
2m	OMe	228–231	0.78	(94%)
2n	OEt	243–247	6.1	n.d.
2o	CO ₂ H	262–265	> 10	n.d.
2p	CONH ₂	264–266	0.93	(94%)
8		258–260	> 10	n.d.
9		> 315	> 10	n.d.

^a Recombinant wild-type human enzyme. Values are means of at least three experiments; standard deviations are ±15%. An IC₅₀ of > 10 indicates that no curve was noted in the dose response up to 10 μM. ^b Values are means of at least three experiments; standard deviations are ±8%. Values in parentheses are percent inhibition ±8% observed at an initial screening concentration of 10 μM. ^c Not determined.

tion, and it was able to detect inhibition of F16BPase by AMP (IC₅₀ = 0.8 μM). Compounds were simultaneously screened for their ability to inhibit recombinant rat liver F16BPase¹⁵ and recombinant porcine kidney F16BPase,¹⁶ as well as purified commercial native rabbit liver F16BPase.¹⁷ In general, the thiazole-substituted anilinoquinazolines were inactive (IC₅₀ values typically ≫ 10 μM) against the rat liver F16BPase. Screening against the porcine kidney F16BPase was conducted to support ongoing crystallographic work using this isoform, while screening against the rabbit isoform was conducted to evaluate the rabbit as a potential animal model. Given the origin of **1** as an inhibitor of the EGFR tyrosine kinase, selected compounds were screened for their ability to inhibit EGFR tyrosine kinase in order to ensure that selectivity for the desired F16BPase target was maintained.¹⁸

SAR

A. Thiazole Ring Substituent (T₂). This portion of the molecule was the first to be explored, as it was quickly found that this substituent could profoundly affect the tyrosine kinase inhibitory activity of these compounds. While **2a** (T₂ = Me) was a relatively modest inhibitor of the EGFR tyrosine kinase (IC₅₀ = 4.8 μM), **2b** (T₂ = H) was much more potent, with an IC₅₀ of 18 nM. This result suggested that the tyrosine kinase inhibitory activity might be eliminated entirely from these compounds by the incorporation of a group sterically larger than methyl. Unfortunately, the SAR at this site proved to be quite narrow (Table 1). Only sterically very small, nonionized residues were tolerated, such as methyl (**2a**), carbinol (**2g**), methoxy (**2m**), and primary

Table 2. Variation of the Pendant Heterocyclic Ring


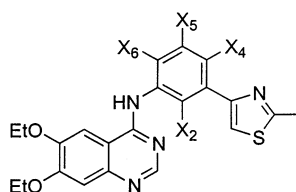
compd	R	mp (°C)	F16BP (IC ₅₀ , μM) ^a	EGFR (IC ₅₀ , μM) ^b
2a	2-Me-4-Tz ^c	259–260	0.64	4.8 (86%)
3a	4-H-2-Tz ^d	251–252	0.38	0.002
3b	4-Me-2-Tz	270–271	0.65	(82%)
3c	4-CONH ₂ -2-Tz	284–286	0.83	(80%)
3d	2-H-5-Tz ^e	264–265	0.98	0.011
3e	2-H-4-Oz ^f	250–251	3.6	0.72
3f	2-Me-4-Oz	272–274	0.50	n.d. ^g
3g	2-Me-5-Oz ^h	276–277	4.0	> 10
3h	3-pyrazolyl	248–249	0.73	0.011
3i	2-pyridyl	262–263	0.39	(100%)
3j	3-pyridyl	255–256	1.4	(97%)
3k	phenyl	258–259	> 10	n.d.
3l	2-tolyl ⁱ	260–261	> 10	n.d.
3m	3-tolyl	250–251	> 10	n.d.
3n	4-tolyl	259–261	> 10	n.d.
3o	2-furyl	241–244	1.4	0.003
3p	3-triazolyl ^j	270–272	0.64	0.39
3q	5-pyrimidyl	276–277	1.2	1.1

^a Recombinant wild-type human enzyme. Values are means of at least three experiments; standard deviations are $\pm 15\%$. An IC₅₀ of > 10 indicates that no curve was noted in the dose response up to 10 μM. ^b Values are means of at least three experiments; standard deviations are $\pm 8\%$. Values in parentheses are percent inhibition $\pm 8\%$ observed at an initial screening concentration of 10 μM. ^c 2-Methyl-4-thiazolyl. ^d 2-Thiazolyl. ^e 5-Thiazolyl. ^f 4-Oxazolyl. ^g Not determined. ^h 2-Methyl-5-oxazolyl. ⁱ (2-Methyl)phenyl. ^j 1,2,4-Triazolyl.

amide (**2p**). While the tyrosine kinase inhibitory potency of some of these compounds was diminished with respect to **2b**, being similar to that of **2a**, this substituent could not be used to incorporate high selectivity for the F16BPase target.

B. Thiazole Regioisomers and Replacements. Replacement of the 2-substituted-4-aryl thiazoles found in **2a,p** by similar 4-substituted-2-aryl thiazoles (**3b,c**) showed that the orientation of the thiazole was not critical for F16BPase inhibitory activity. Other five-membered heterocycles such as pyrazole (**3h**), oxazole (**3f**), furan (**3o**), and triazole (**3p**) were active with F16BPase potencies of IC₅₀ = 0.5–2 μM (Table 2). Enlargement of the heterocyclic ring to a six-membered ring was also investigated. Again, a variety of heterocycles were found to be tolerated, such as the pyridyl analogues **3i,j** and the pyrimidine **3q**. To our surprise, however, substitution of a phenyl ring, with or without additional methyl substituents (**3k–n**), in place of the thiazole or pyridine rings eliminated F16BPase activity. The X-ray crystallographic studies (vide infra) suggest that **3k–n** may be unable to coordinate to water molecules found in the bound conformation. This position could not be used to introduce selectivity for F16BPase inhibition, as significant EGFR tyrosine kinase inhibition accompanied the F16BPase inhibition.

C. Additional Phenyl Ring Substituents. Replacement of the hydrogens on this ring was generally found to reduce potency. Addition of a fluorine atom ortho (**4b**) or para (**4d**) to the thiazole ring was tolerated, but no substantial improvement in potency was observed (Table 3). When both positions were substituted by fluorine

Table 3. Variation of Phenyl Ring Substituents


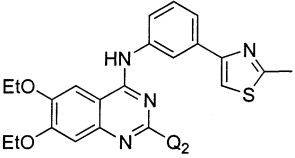
compd	X ₂	X ₄	X ₅	X ₆	mp (°C)	F16BP (IC ₅₀ , μM) ^a	EGFR (IC ₅₀ , μM) ^b
2a	H	H	H	H	259–260	0.64	4.8
4a	H	H	CF ₃	H	282–283	> 10	n.d. ^c
4b	H	F	H	H	280–281	0.61	(84%)
4c	H	Cl	H	H	275–276	5.3	n.d.
4d	H	H	H	F	267–268	0.48	(73%)
4e	H	H	H	Cl	261–262	1.7	n.d.
4f	H	F	H	F	280–282	> 10	n.d.
4g	H	H	H	Me	231–232	1.8	(69%)
4h	H	H	H	OMe	194–197	0.99	n.d.
4i	H	H	H	OEt	164–167	1.8	(90%)
4j	H	H	H	Br	234–237	> 10	n.d.
4k	H	H	H	Et	179–181	2.1	n.d.
4l	F	F	H	H	236–240	> 10	n.d.

^a Recombinant wild-type human enzyme. Values are means of at least three experiments; standard deviations are $\pm 15\%$. An IC₅₀ of > 10 indicates that no curve was noted in the dose response up to 10 μM. ^b Values are means of at least three experiments; standard deviations are $\pm 8\%$. Values in parentheses are percent inhibition $\pm 8\%$ observed at an initial screening concentration of 10 μM. ^c Not determined.

(**4f**), enzyme inhibitory activity was lost. Similarly, placement of two fluorine substituents ortho to the thiazole ring eliminated activity (**4l**). As the results with **4f,l** are difficult to rationalize in terms of steric effects, we presume this to be the result of a diminished ability of **4f,l** to participate in the π -stacking found in the X-ray crystal structure due to the electronic perturbation of the phenyl ring brought about by the presence of the two fluorine atoms. Some relatively small substituents para to the thiazole ring, such as methyl (**4g**) or methoxy (**4h**), gave analogues with diminished F16BPase inhibitory potency. Not surprisingly, the EGFR counter assay at 10 μM concentration of selected compounds from this group revealed that they retained considerable EGFR tyrosine kinase inhibitory activity.

D. Quinazoline 2-Position. In contrast to the relatively narrow requirements of the thiazole substituent and the isolated phenyl ring, a wide variety of substituents could be incorporated at the quinazoline 2-position while retaining F16BPase inhibitory activity (Table 4). Many hydrophilic groups, whether neutral (**5l**), basic (**5n**), or acidic (**5r**), were all tolerated, which suggested that perhaps these groups were solvent-exposed. In contrast, a large hydrophobic group, such as benzyl (**5e**), was not tolerated. Basic substituents such as **5n,p,s,t** were found to have the derivative benefit of improving aqueous solubility.

Of even greater interest was the observation that all of the groups that were examined at this position except methyl (**5a**) and ethyl (**5b**) largely eliminated the EGFR tyrosine kinase inhibitory activity. This separation of the two enzyme inhibitory activities was particularly gratifying in light of the restrictive SAR results obtained at other sites on these compounds, in which the F16BPase inhibitory activity was more or less subsumed within a more potent EGFR tyrosine kinase inhibition

Table 4. Variation of Substituents at Quinazoline 2-Position


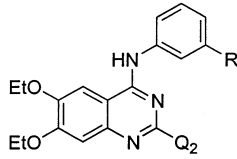
compd	Q ₂	mp (°C)	F16BP (IC ₅₀ , μM) ^a	EGFR (IC ₅₀ , μM) ^b
2a	H	259–260	0.64	4.8
5a	Me	249–250	1.0	9.0
5b	Et	243–244	1.5	9.3
5c	<i>n</i> -C ₃ H ₇	239–240	1.4	(20%) ^c
5d	<i>i</i> -C ₃ H ₇	188–190	5.0	(23%)
5e	CH ₂ Ph	249–250	>10	n.d. ^d
5f	Cl	146–149	2.6	n.d.
5g	CH ₂ Cl	252–256	0.87	(10%)
5h	(CH ₂) ₂ Cl	229–230	1.0	(11%)
5i	(CH ₂) ₃ Cl	185–188	4.1	(31%)
5j	CF ₃	165–171	>10	n.d.
5k	CH ₂ SO ₂ Me	248–251	2.1	(10%)
5l	CH ₂ OMe	141–143	1.4	(17%)
5m	CH ₂ NH ₂	115–118	1.5	(0%)
5n	CH ₂ NMe ₂	170–172	2.0	(12%)
5o	CH ₂ NHEt	235–237	6.0	(0%)
5p	CH ₂ N(CH ₂) ₄	232–235	6.1	(8%)
5q	CH ₂ CHMe ₂	230–232	1.7	(12%)
5r	CH ₂ CO ₂ H	158–160 ^e	0.96	(21%)
5s	CH ₂ C ₃ H ₃ N ₂ ^f	207–210	0.77	(38%)
5t	CH ₂ CH ₂ NH ₂	219–222	0.22	(18%)

^a Recombinant wild-type human enzyme. Values are means of at least three experiments; standard deviations are ±15%. An IC₅₀ of >10 indicates that no curve was noted in the dose response up to 10 μM. ^b Values are means of at least three experiments; standard deviations are ±8%. Values in parentheses are percent inhibition ±8% observed at an initial screening concentration of 10 μM. ^c Inhibition ≤20% is not significant. ^d Not determined. ^e Decomposes. ^f 1-Imidazolyl.

SAR. While the degree of separation between these two activities required for success in vivo is unclear, the separation obtained with compounds such as **5m,n,t** offers a degree of selectivity for F16BPase inhibition previously unattained with anilinoquinazoline inhibitors.

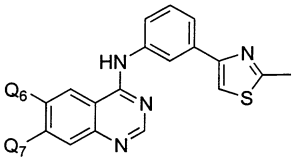
The relatively permissive SAR observed at this position was remarkable in light of the very restrictive requirements previously observed for the quinazoline 2-position in the halogen-substituted anilinoquinazolines **1**.¹⁹ Halogen- and alkyne-substituted anilinoquinazolines such as **1** were found to tolerate only H and methyl at the quinazoline 2-position. Indeed, side by side comparisons of quinazoline 2-positions substituents with either bromine or thiazole substituents on the phenyl ring revealed that the requirements for the quinazoline 2-position were in fact divergent (Table 5). These results suggest, but do not prove, that the binding modes for anilinoquinazolines substituted with heterocyclic rings and those substituted with halogens or alkyne residues are different despite their structural similarity.

E. Quinazoline Benzo Ring Substituents. A preference for a 6,7-diethoxy or 6-ethoxy-7-isopropoxy substitution pattern was noted (Table 6). This was observed with varying combinations of methoxy, ethoxy, butoxy, and (2-methoxy)ethoxy substituents (MEE) at the 6- and 7-positions. These results were in contrast to those observed previously for the halogen-substituted anilinoquinazolines **1**, in which a preference for a 6,7-

Table 5. Effect of Thiazolyl vs Bromo Phenyl Ring Substituents in 2-Substituted Quinazolines


compd	Q ₂	R	mp (°C)	F16BP (IC ₅₀ , μM) ^a
5g	CH ₂ Cl	2-Me-4-Tz	252–256	0.87
5k	CH ₂ SO ₂ Me	2-Me-4-Tz	248–251	2.1
5q	CH ₂ CHMe ₂	2-Me-4-Tz	230–232	1.7
5u	CH ₂ Cl	Br	273–276	>10
5v	CH ₂ SO ₂ Me	Br	267–268	>10
5w	CH ₂ CHMe ₂	Br	252–254	>10

^a Recombinant wild-type human enzyme. Values are means of at least three experiments; standard deviations are ±15%. An IC₅₀ of >10 indicates that no curve was noted in the dose response up to 10 μM.

Table 6. Variation of Substituents at Quinazoline 6- and 7-Positions


compd	Q ₆	Q ₇	mp (°C)	F16BP (IC ₅₀ , μM) ^a	EGFR (IC ₅₀ , μM) ^b
2a	EtO	EtO	259–260	0.64	4.8
6a	H	H	245–246	>10	n.d. ^c
6b	MeO	MeO	257–258	4.4	n.d.
6c	MeO	EtO	259–261	3.4	n.d.
6d	MeO	<i>n</i> -PrO ^d	252–253	5.6	n.d.
6e	MeO	<i>i</i> -PrO ^e	259–260	2.3	n.d.
6f	MeO	<i>n</i> -BuO ^f	259–260	>10	n.d.
6g	MeO	<i>s</i> -BuO ^g	222–224	1.3	(87%)
6h	MeO	<i>i</i> -BuO ^h	255–258	>10	n.d.
6i	MeO	MEE ⁱ	252–253	>10	n.d.
6j	MeO	<i>c</i> -Pn ^j	259–260	>10	n.d.
6k	EtO	MeO	252–253	1.2	n.d.
6l	<i>i</i> -PrO	MeO	232–234	>10	n.d.
6m	<i>n</i> -BuO	MeO	240–241	>10	n.d.
6n	MEE	MeO	237–239	>10	n.d.
6o	EtO	<i>n</i> -PrO	238–241	1.0	(83%)
6p	EtO	<i>i</i> -PrO	257–259	0.42	(90%)
6q^k	EtO	EtO	174–177	>10	n.d.
6r	OCH ₂ CH ₂ O		>280	>10	n.d.
6s	CH=CH–CH=CH		278–281	>10	n.d.

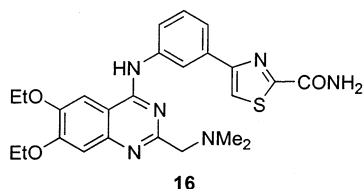
^a Recombinant wild-type human enzyme. Values are means of at least three experiments; standard deviations are ±15%. An IC₅₀ of >10 indicates that no curve was noted in the dose response up to 10 μM. ^b Values are means of at least three experiments; standard deviations are ±8%. Values in parentheses are percent inhibition ±8% observed at an initial screening concentration of 10 μM. ^c Not determined. ^d *N*-propyloxy, CH₃CH₂CH₂O. ^e *Iso*-propyloxy, (CH₃)₂CHO. ^f *N*-butyloxy, CH₃(CH₂)₃O. ^g *Sec*-butyloxy, (CH₃)(C₂H₅)CHO. ^h *Isobutyloxy*, (CH₃)₂CHCH₂O. ⁱ (2-Methoxy)ethoxy, MeOCH₂CH₂O. ^j Cyclopentyloxy, C₅H₉O. ^k 6,7,8-Triethoxy.

dimethoxy substitution pattern was observed. Incorporation of an alkoxy group at the quinazoline 8-position abolished activity (**6q**). Incorporation of the alkoxy groups into a ring (**6r**) or fusion of another benzo ring (**6s**) likewise resulted in the loss of F16BPase inhibition. Functional groups other than alkoxy groups at the quinazoline 6- and 7-positions afforded inactive analogues.²⁰ The EGFR tyrosine kinase inhibition SAR at

this part of the molecule was not investigated extensively. EGFR counter assay at 10 μM concentration of those analogues with the best F16BPase inhibitory potencies revealed that these compounds also had significant EGFR tyrosine kinase inhibitory activity; therefore, selectivity was unlikely to be introduced by modifying this position.

Mode of Binding

To better understand the binding mode of our compounds, we cocrystallized recombinant porcine kidney F16BPase with **16** ($\text{IC}_{50} = 2.4 \mu\text{M}$ human, $9.5 \mu\text{M}$ pig) in the presence of manganous chloride, AMP, and fructose-6-phosphate (see Experimental Section). The choice of **16** was based on its high water solubility ($>250 \mu\text{g mL}^{-1}$). These crystals were found to contain **16** at a novel binding site at the subunit interface. While the protein crystal structure was resolved to 2.0 Å, the density map of **16** within the binding site was not of sufficiently high resolution to identify all contacts between the inhibitor and the enzyme. This is presumed to be due to the relatively low potency of **16** against the porcine isoform. Accordingly, a more potent inhibitor, **2g** ($\text{IC}_{50} = 0.83 \mu\text{M}$ human and pig), was subsequently soaked into these crystals.



Our structure reveals a novel binding site for **2g** at the subunit interface, distinct from the known allosteric and substrate sites, which are occupied by AMP and F6P, respectively (Figure 1). Two crystal-symmetry-related molecules of the inhibitor occupy a shallow channel formed at the interface between two subunits of the protein (Figure 2). This site is normally filled with water and retains water below the bound molecules of **2g** after binding has occurred. The subunits are found to have rotated by 17° from their position in the catalytically active R state, in the same manner as is observed in the AMP-inhibited T state structure. The inhibitor molecules stack against one another in a head-to-tail fashion and are π -stacked to the imidazole rings of symmetry-related side chains of His 55 (Figure 3). A hydrogen bond appears to be made through a water molecule from the side chain of Lys 50 to the oxygen atoms of the ortho-diethoxy groups. A second hydrogen bond through water appears to be made from quinazoline N1 to the backbone NH of Lys 71, while the quinazoline ring itself makes hydrophobic contacts to the side chains of Leu 56 and Val 70. No direct hydrogen bonds appear to occur at allowable distances between **2g** and His 55. Also of note are two organized water molecules per compound between the NH and the thiazole ring nitrogen. The organization of these water molecules may explain the observation that biphenyl analogues such as **3k** were inactive. Furthermore, alkylation of the aniline nitrogen atom, to afford the N-methyl derivative **17**, was found to eliminate F16BPase



Figure 1. Ribbon diagram of T state porcine kidney F16BPase homotetramer showing the bound ligands AMP, fructose 6-phosphate, and **2g**. The individual enzyme subunits are colored differently.

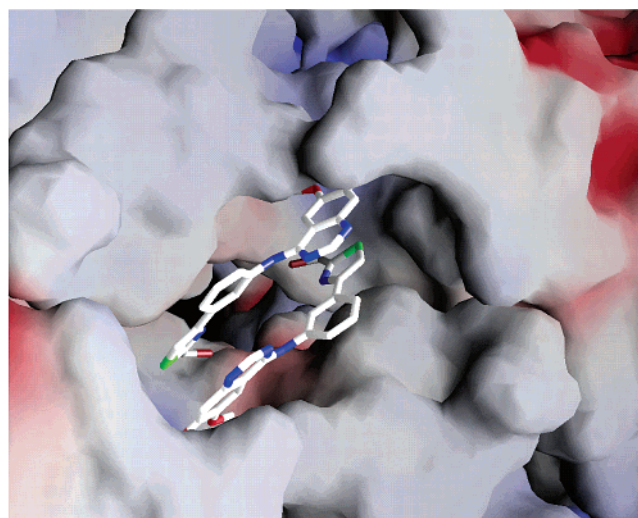
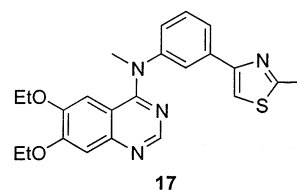


Figure 2. X-ray crystal structure of **2g** bound to porcine kidney F16BPase at the homotetramer subunit interface.

inhibitory activity. The hydroxyl residue in **2g** makes a hydrogen bond contact to a backbone carbonyl group of Ala 51 as well. The quinazoline 2-substituent was shown to be solvent-exposed, as the experimental SAR had suggested.



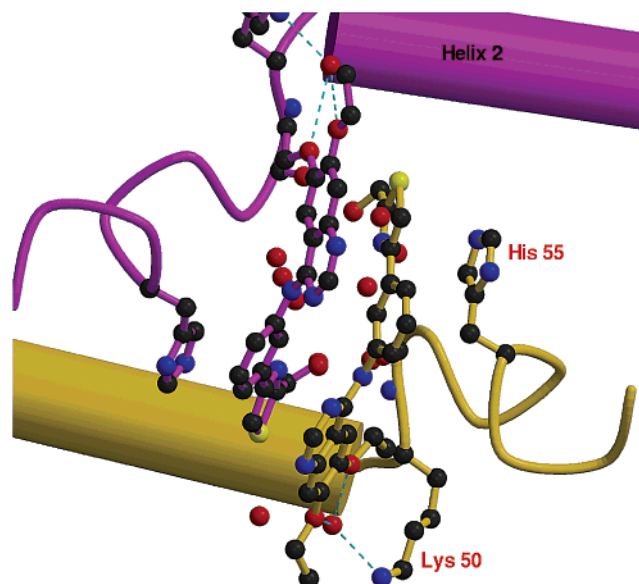


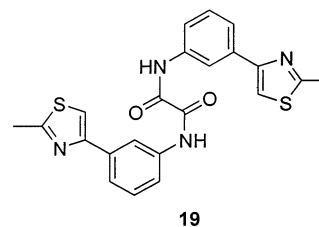
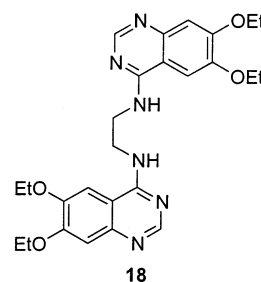
Figure 3. Schematic diagram of **2g** bound to porcine kidney F16BPase showing key recognition contacts made to Lys 50 and His 55.

Conformational changes in loops 52–72 have been shown to be involved in regulating the transition from the catalytically active R state to the inactive T state in F16BPase.²¹ This loop interacts with the active site of its own subunit in the R state to assemble the catalytic site. Asp 68 participates in the coordination of zinc required for catalysis. The loop pivots between the different conformational states about a “hinge” at Lys 50 and Ala 51,²² which has been shown to be a critical element at the C1–C2 subunit interface for cooperative AMP binding.²³

By contrast, parts or all of this loop are disordered in all published crystal structures of the T state enzyme, including this one, where no density is seen for residues 62–69. A mechanism of allosteric regulation by AMP has been presented in which AMP, by binding to its allosteric pocket, displaces loops 52–72 from the catalytic site resulting in disassembly of the structural elements necessary for catalysis. Movement of the loop into the disengaged conformation, and the consequent rotation about the hinge region, results in the overall quaternary conformational changes associated with the R state to T state transition.²⁴ It is likely that the inhibitor **2g**, by binding to Lys 50 in the hinge region and to residues 55, 56, 70, and 71 in the loop, likewise stabilizes this disengaged conformation and thus keeps the enzyme in the T state.

The head-to-tail stacking of the inhibitor molecules against one another may be responsible in part for the inability to secure a significant potency improvement with this series, as a significant amount of the binding “pocket” for any particular inhibitor molecule is composed of another molecule of inhibitor. However, the close proximity of the two inhibitor molecules at the binding site may serve as a point of departure for further inhibitor design. A single molecule that can act at this site to block assembly of the catalytic site would be expected to be significantly more potent.²⁵ A simple linking of the two inhibitor molecules through the quinazoline 2-position is possible based on this X-ray structure, but such a compound would be unlikely to

have acceptable druglike physicochemical properties.²⁶ A symmetric compound that makes both of the π -stacking interactions with His 55 or both of the hydrogen-bonding interactions with Lys 50 would be more likely to fall within the range of acceptable physicochemical properties, and the design of such a molecule represents an opportunity for computational chemistry. The results of the mutagenesis studies (vide infra) suggest that the interactions with His 55 may be of greater significance than the interactions with Lys 50. The bis-quinazoline **18** or bis-phenylthiazole **19** may serve to help illustrate this concept.²⁷



Attempts to crystallize the human enzyme²⁸ with these compounds have been unfruitful as the crystals obtained to date have a very large unit cell that is difficult to work with. A solution molecular weight experiment performed on the human enzyme showed that the molecular weight of the human enzyme increased by about 1700 mass units, corresponding to the incorporation of 4 equiv of **2g** with a molecular weight of 422.

Mutagenesis Studies

The degree of amino acid sequence conservation within the F16BPase coding region among mammalian species is very high (>90% identity). However, sequence comparisons at the novel binding site identified above show that the critical Lys 50 and His 55 residues are conserved among pig, rabbit, and human isoforms. In contrast to these three species, the rat and mouse encode glutamine at both positions. All other amino acids within the loop and hinge region are conserved among these five species. Glutamine would be expected to be entirely unable to make the key hydrogen bonds (Lys50) and π -stacking bonds (His55) that are seen in the porcine kidney enzyme X-ray structure and would be predicted to sterically block the binding of our compounds as well. These changes to glutamine in the rat liver enzyme are likely responsible for the observed lack of inhibition of the rat liver enzyme. To test this hypothesis, we prepared Gln50His and Gln55His single-site mutant derivatives of the rat enzyme as well as the Gln50Lys, Gln55His double mutant. Each was expressed in and purified from the *Escherichia coli* strain BL21(DE3) as the wild-type rat and human isoforms

Table 7. Directed Mutagenesis Results

compd	F16BPase (IC ₅₀ , μM) ^a				rat (wild-type)
	human (wild-type)	Gln50Lys ^b Gln55His	Gln50Lys ^c	Gln55His ^d	
2a	0.64	0.79	>10	3.8	>10
2g	0.83	0.34	>10	2.9	>10
2p	0.93	0.52	>10	3.0	>10

^a Values are means of at least three experiments; standard deviations are ±0.25 μM. An IC₅₀ of >10 indicates that no curve was noted in the dose response up to 10 μM. ^b Recombinant Gln 50 to Lys 50; Gln 55 to His 55 rat double mutant enzyme. ^c Recombinant Gln 50 to Lys 50 rat single mutant enzyme. ^d Recombinant Gln 55 to His 55 rat single mutant enzyme.

were. The catalytic competency of the mutant enzymes was confirmed by showing that the specific activities of the three mutants and the wild-type rat enzyme were the same. Each of the five isoforms of F16BPase was tested for its activity in the presence of **2a,g,p** using the malachite green assay. The IC₅₀ values are shown in Table 7. As seen previously, the thiazole-substituted anilinoquinazolines were potent inhibitors of the human enzyme yet completely inactive against the wild-type rat isoform (IC₅₀ values ≫ 10 μM). Interestingly, the mutant series displayed a gradation of increasing potency. Gln50Lys was still unaffected by these inhibitors, while the Gln55His single site variant was inhibited to a moderate degree. The combination of these changes in the Gln50Lys, Gln55His enzyme resulted in IC₅₀ values comparable to those seen with the human enzyme. These results support the hypothesis that Lys 50 and particularly His 55 are the key amino acid residues required for inhibitor recognition and binding.

Summary

Thiazole-containing anilinoquinazolines such as **2–6** represent novel, low molecular weight (<500) inhibitors of F16BPase that are not substrate mimics or AMP analogues. Unlike the anilinoquinazolines **1** previously described as F16BPase inhibitors, compounds with hydrophilic substituents at the quinazoline 2-position (**5**) are selective inhibitors of F16BPase that lack the EGFR tyrosine kinase inhibitory activity associated with **1** and have a different SAR profile than **1** and its analogues, implicating different binding modes for **1–6**. The solvent-exposed substituent at the quinazoline 2-position also permits modification of physical chemical properties that was not possible with the anilinoquinazolines such as **1**. At other sites, the SAR for F16BPase inhibition and EGFR tyrosine kinase inhibition are largely parallel (**2–4** and **6**). The compounds bind as head-to-tail π-stacked dimers at a novel C2 symmetric allosteric binding site at the interface of the C1 and C2 subunits. This binding is repeated by symmetry by reflection through a plane on the opposite side of the enzyme. The key residues involved in inhibitor binding have been identified, with the π-stacking interaction with His 55 being of special significance. Inhibition appears to be affected by steric blockade of the assembly of the catalytic site upon compound binding. Studies are in progress to elucidate their in vivo biological properties, particularly their effects upon models of hyperglycemic disease.

Experimental Section

¹H NMR spectra were recorded on Varian Unity Inova 400 MHz spectrometers. Mass spectral data were recorded on Micromass Platform 2 or Hewlett-Packard model 5989 instruments using the indicated ionization techniques. Melting points were determined on a Thomas–Hoover melting point apparatus and are uncorrected. Elemental analyses were performed by Schwarzkopf Microanalytical Laboratory, Woodside, NY, and were within 0.4% of the calculated values. Thin-layer chromatography was carried out with E. Merck 15327 silica gel plates.

All reactions were carried with continuous magnetic stirring under an atmosphere of dry nitrogen. All solutions were dried over anhydrous magnesium sulfate unless otherwise noted; all evaporations were carried out on a rotary evaporator at ca. 30 Torr. Commercial reagents were used as received without additional purification. Solvents were commercial anhydrous grades and were used without further drying. All final products were characterized by ¹H NMR, API MS, melting point, and combustion analysis.

Rabbit liver fructose-1,6-bisphosphatase, fructose-1,6-bisphosphate, and all buffer and detection reagents were obtained from Sigma. Porcine kidney fructose-1,6-bisphosphatase was obtained from Dr. Evan Kantrowitz (Boston College). Recombinant human liver and recombinant rat liver fructose-1,6-bisphosphatase were prepared as described.²⁹ All enzymes were purified to >95% purity. Briefly, purification was effected a dialysis step followed by High-Load SP Sepharose HP, a second lengthy dialysis step, Mono-S, and then, Superdex-75. The quality of the final products was then evaluated by enzyme activity assay, sodium dodecyl sulfate polyacrylamide gel electrophoresis (SDS–PAGE), N-terminal analysis, static and dynamic light scattering, and electrospray mass spectrometry.

4-Chloro-6,7-diethoxyquinazoline (7). **Step 1. 4,5-Diethoxy-2-nitrobenzoic Acid Ethyl Ester (12).** A solution of 50 g (0.21 mol) of 3,4-diethoxybenzoic acid ethyl ester³⁰ in 220 mL of glacial acetic acid was stirred at room temperature while concentrated nitric acid (*d* = 1.42, 70%, 80 mL) was added dropwise. The mixture was cooled as needed with a bath of cold water to maintain the temperature below 30 °C. The mixture was stirred for an additional 3 h, and then, was poured into 1 L of ice water. The precipitate was extracted twice with dichloromethane. The dichloromethane extracts were combined and washed twice with water and then with 1 M sodium bicarbonate until the washes were of pH 8. The dichloromethane extracts were dried and concentrated to afford 59 g (100%) of **12** as colorless crystals; mp 53–54 °C. ¹H NMR (CDCl₃): δ 7.42 (s, 1 H); 7.03 (s, 1 H); 4.35 (q, 2 H); 4.16 (overlapping q, 4 H); 1.48 (overlapping q, 6 H); 1.33 (t, 3 H). MS (EI): *m/z* 283 (M⁺). Anal. (C₁₃H₁₇NO₆): C, H, N.

Step 2. 2-Amino-4,5-diethoxybenzoic Acid Ethyl Ester (13). A solution of 15.7 g (55 mmol) of **12** was hydrogenated at 25 °C under 50 psi in ethanol (350 mL) over 1.00 g of 10% palladium on carbon until the uptake of hydrogen ceased. The mixture was then filtered and concentrated to afford 13.8 g (100%) of **13**; mp 69–71 °C. ¹H NMR (CDCl₃): δ 7.34 (s, 1 H); 6.12 (s, 1 H); 4.28 (q, 2 H); 3.98 (overlapping q, 4 H); 1.43 (t, 3 H); 1.34 (overlapping t, 6 H). MS (API): *m/z* 254 (M + H⁺). Anal. (C₁₃H₁₉NO₄): C, H, N.

Step 3. 4-Chloro-6,7-diethoxyquinazoline (7). A solution of 10.13 g (40 mmol) of **13** and 6.14 g of powdered ammonium carbonate (64 mmol) in 40 mL of formamide was heated to 170 °C over 1 h and then kept at 170 °C for 3 h. The mixture was cooled and poured into 120 mL of water. The precipitate that formed was filtered, washed with water, and dried to afford 8.45 g (90%) of 6,7-diethoxy-3H-quinazolin-4-one as a white solid; mp 255–257 °C (lit.³¹ mp 253–255 °C). ¹H NMR (DMSO-*d*₆): δ 7.93 (s, 1 H); 7.38 (s, 1 H); 7.07 (s, 1 H); 4.13 (q, 2 H); 4.08 (q, 2 H); 1.35 (overlapping t, 6 H). MS (API): *m/z* 235 (M + H⁺). This was dissolved in 50 mL of phosphorus oxychloride and heated at reflux for 2 h. The mixture was then cooled and concentrated to a small volume. The residue was added to a solution of 120 g of sodium carbonate in 300 mL of water and 300 mL of ethyl acetate. The mixture was stirred

for 15 min, and then, the ethyl acetate was washed with brine, dried, and concentrated. The residue was crystallized from 1-chlorobutane to give 8.02 g (88%) of **7**; mp 141–143 °C (lit.²⁶ mp 140–141 °C). ¹H NMR (CDCl₃): δ 8.83 (s, 1 H); 7.36 (s, 1 H); 7.30 (s, 1 H); 4.27 (overlapping q, 4 H); 1.56 (overlapping t, 6 H). MS (API): *m/z* 253, 255 (M + H⁺, Cl isotope pattern). Anal. (C₁₂H₁₃ClN₂O₂): C, H, N.

3-(2-Methyl-thiazol-4-yl)phenylamine (15). A solution of 12.20 g (50 mmol) of 3-nitrophenacyl bromide in 100 mL of ethanol was heated to reflux and then treated with 6.01 g (80 mmol) of thioacetamide added in four portions. Heating was continued for 90 min, and then, the mixture was allowed to cool. The precipitate that formed was filtered, washed with ethanol, and dried to afford 9.19 g (83%) of 2-methyl-4-(3-nitrophenyl)-thiazole; mp 102–104 °C (lit.³² mp 104 °C). ¹H NMR (DMSO-*d*₆): δ 8.70 (s, 1 H); 8.35 (d, 1 H); 8.23 (s, 1 H); 8.14 (d, 1 H); 7.69 (t, 1 H); 2.71 (s, 3 H). MS (API): *m/z* 221 (M + H⁺). This was added in three portions over 10 min to a refluxing solution of tin(II) chloride dihydrate (31.05 g, 0.137 mol) in ethanol (100 mL) and concentrated hydrochloric acid (50 mL). Heating was continued for 20 min longer, and then, the solution was cooled and poured into a cold solution of 120 g of potassium hydroxide in 1 L of water with stirring. Stirring with ice cooling was continued for 15 min, and then, the precipitate was filtered, washed with water, and dried to afford 6.87 g (86%) of **15**; mp 102–103 °C (lit.³³ mp 80–81, 88–90, 134–137 °C). ¹H NMR (CDCl₃): δ 7.25 (m, 2 H); 7.20 (m, 2 H); 6.66 (d, 1 H); 2.75 (s, 3 H). MS (API): *m/z* = 191 (M + H⁺). Anal. (C₁₀H₁₀N₂S): C, H, N.

(6,7-Diethoxy-quinazolin-4-yl)-[3-(2-phenyl-thiazol-4-yl)phenyl]amine (2e, Scheme 1). **Step 1. 1-[3-(6,7-Diethoxy-quinazolin-4-ylamino)phenyl]ethanone (8).** A solution of 4.30 g (16.9 mmol) of **7** in 80 mL of 2-propanol was heated at reflux and treated with 2.51 g (18.6 mmol) of 3-aminoacetophenone added in a single portion. Heating was continued for 1 h, after which the reaction mixture was allowed to cool. The precipitated product was filtered, washed with 2-propanol, and dried to afford 5.19 g (87%) of the title product; mp 258–260 °C. ¹H NMR (DMSO-*d*₆): δ 8.81 (s, 1 H); 8.18 (m, 2 H); 7.97 (d, 1 H); 7.88 (d, 1 H); 7.62 (t, 1 H); 7.27 (s, 1 H); 4.24 (overlapping q, 4 H); 2.59 (s, 3 H); 1.43 (overlapping t, 6 H). MS (API): *m/z* 352 (M + H⁺). Anal. (C₂₀H₂₁N₃O₃·HCl): C, H, N.

Step 2. 2-Bromo-1-[3-(6,7-diethoxy-quinazolin-4-yl-amino)phenyl]ethanone (9). A solution of 3.53 g (10 mmol) of **8** in 45 mL of acetic acid and 15 mL of 48% hydrobromic acid was heated to reflux and treated with 10 mL of a 1 M solution of bromine in acetic acid. After 20 min, the color had been discharged and the reaction was cooled and filtered to afford 2.79 g (65%) of **9**; mp >315 °C. ¹H NMR (DMSO-*d*₆): δ 8.84 (s, 1 H); 8.20 (s, 1 H); 8.06 (s, 1 H); 7.97 (m, 2 H); 7.66 (t, 1 H); 7.22 (s, 1 H); 4.95 (s, 2 H); 4.25 (overlapping q, 4 H); 1.43 (overlapping q, 6 H). MS (API): *m/z* 430, 432 (M + H⁺). Anal. (C₂₀H₂₀BrN₃O₃·HBr): C, H, N.

Step 3. (6,7-Diethoxy-quinazolin-4-yl)-[3-(2-phenyl-thiazol-4-yl)phenyl]amine (2e). A mixture of 0.432 g (1.0 mmol) of **9** and 0.137 g (1.0 mmol) of thiobenzamide in 15 mL of ethanol was heated at reflux for 2 h. The reaction mixture was filtered while still hot. The precipitate was washed with ethanol and dried to afford 0.343 g (73%) of **2e**; mp 274–275 °C. ¹H NMR (DMSO-*d*₆): δ 8.82 (s, 1 H); 8.25 (m, 2 H); 8.09 (s, 1 H); 8.02 (m, 3 H); 7.67 (d, 1 H); 7.58 (t, 1 H); 7.50 (m, 3 H); 7.21 (s, 1 H); 4.24 (overlapping q, 4 H); 1.43 (overlapping q, 6 H). MS (API): *m/z* 469 (M + H⁺). Anal. (C₂₇H₂₄N₄O₂S·HBr): C, H, N.

4-[3-(6,7-Diethoxy-quinazolin-4-ylamino)phenyl]thiazole-2-carboxylic Acid Amide (2p, Scheme 2). **Step 1. 4-(3-Nitrophenyl)thiazole-2-carboxylic Acid Ethyl Ester (10).** A solution of 3-nitrophenacyl bromide (13.34 g, 55 mmol) in 80 mL of ethanol was heated at reflux and treated with ethyl thioacetate (7.28 g, 55 mmol). Heating was continued for 40 min, after which the reaction mixture was allowed to cool. The precipitated product was filtered, washed with ethanol, and dried to afford 12.64 g (83%) of **10**; mp 149–150

°C. ¹H NMR (CDCl₃): δ 8.75 (m, 1 H); 8.31 (d of t, 1 H); 8.20 (d of t, 1 H); 7.89 (s, 1 H); 7.62 (t, 1 H); 4.49 (q, 2 H); 1.46 (t, 3 H). MS (EI): *m/z* 278 (M⁺). Anal. (C₁₂H₁₀N₂O₄S): C, H, N.

Step 2. 4-(3-Aminophenyl)thiazole-2-carboxylic Acid Amide (11). A solution of tin(II) chloride dihydrate (1.331 g, 5.9 mmol) in ethanol (10 mL) and concentrated hydrochloric acid (1.8 mL) was heated to reflux and treated with **10** (0.500 g, 1.8 mmol). Heating was continued for 40 min, after which the reaction mixture was cooled and poured into a solution of 4.0 g of potassium hydroxide in 50 mL of water with ice cooling. The precipitated product was extracted with ethyl ether. The ether extract was washed with water and brine, dried, and concentrated to afford 0.266 g (60%) of 4-(3-aminophenyl)thiazole-2-carboxylic acid ethyl ester as a viscous syrup. ¹H NMR (CDCl₃): δ 7.68 (s, 1 H); 7.35 (m, 1 H); 7.21 (m, 2 H); 6.69 (d of t, 1 H); 4.48 (q, 2 H); 1.43 (t, 3 H). MS (API): *m/z* 249 (M + H⁺). This was dissolved in 15 mL of ethanol, and the solution was saturated with dry ammonia gas with cooling in ice. The mixture was tightly stoppered and stirred at room temperature overnight. The reaction mixture was concentrated to dryness to afford 0.223 g (92%) of **11**; mp 193–194 °C. ¹H NMR (DMSO-*d*₆): 8.16 (s, 1 H); 8.13 (br, 1 H); 7.93 (br, 1 H); 7.22 (m, 2 H); 7.14 (t, 1 H); 6.59 (d of t, 1 H); 5.18 (br, 2 H). MS (API): *m/z* 220 (M + H⁺). Anal. (C₁₀H₉N₃OS): C, H, N.

Step 3. 4-[3-(6,7-Diethoxy-quinazolin-4-ylamino)phenyl]thiazole-2-carboxylic Acid Amide (2p). A solution of 0.157 g (0.62 mmol) of **7** in 2.5 mL of ethanol was heated at reflux and treated with 0.136 g (0.62 mmol) of **11** dissolved in 4 mL of ethanol added in a single portion. Heating was continued for 30 min, after which the reaction mixture was allowed to cool. The precipitated product was filtered, washed with ethanol, and dried to afford 0.152 g (56%) of **2p**; mp 264–266 °C. ¹H NMR (DMSO-*d*₆): δ 11.40 (s, 1 H); 8.79 (s, 1 H); 8.42 (d, 1 H); 8.28 (s, 1 H); 8.24 (s, 1 H); 7.99 (d, 1 H); 7.93 (s, 1 H); 7.62 (m, 1 H); 7.55 (m, 1 H); 7.32 (m, 1 H); 4.23 (overlapping q, 4 H); 1.41 (overlapping t, 6 H). MS (API): *m/z* 436 (M + H⁺). Anal. (C₂₂H₂₁N₅O₃S·HCl): C, H, N.

(6,7-Diethoxy-quinazolin-4-yl)-(3-pyridin-3-yl-phenyl)-amine (3j). **Step 1. 3-(3-Nitrophenyl)pyridine.** This compound was prepared by a modification of that previously reported. A mixture of 0.417 g (2.5 mmol) of 3-nitrophenylboronic acid, 0.355 g (2.2 mmol) of 3-bromopyridine, 0.435 g (7.5 mmol) of potassium fluoride, and 0.087 g (0.075 mmol) of tetrakis(triphenylphosphine) palladium(0) in 10 mL of 95% ethanol was heated at reflux for 18 h. The reaction mixture was cooled and poured into 2 M potassium hydroxide and extracted with ethyl ether. The ether was washed with water and brine, dried, and concentrated. The residue was recrystallized from 2-propanol to afford 0.197 g (44%) of 3-(3-nitrophenyl)pyridine; mp 100–102 °C (lit.³⁴ mp 101–102). ¹H NMR (CDCl₃): δ 8.91 (t, 1 H); 8.67 (m, 1 H); 8.45 (t, 1 H); 8.29 (d of t, 1 H); 8.02 (d, 1 H); 7.91 (m, 1 H); 7.68 (m, 1 H); 7.50 (m, 1 H). MS (EI): *m/z* 200 (M⁺).

Step 2. 3-Pyridin-3-yl-phenylamine. A solution of 0.744 g (3.3 mmol) of tin(II) chloride dihydrate in 6 mL of ethanol and 1 mL of concentrated hydrochloric acid was heated to reflux and treated with 0.197 g (0.98 mmol) of 3-(3-nitrophenyl)pyridine. Heating was continued for 0.5 h, after which the reaction mixture was cooled and poured into a solution of 5.0 g of potassium hydroxide in 30 mL of water with ice cooling. The mixture was extracted with ethyl ether. The ether was washed with water and brine, dried, and concentrated to afford 0.141 g (84%) of 3-pyridin-3-yl-phenylamine as a viscous oil that crystallized on standing; mp 70–72 °C (lit.³⁵ mp 72–74 °C). ¹H NMR (CDCl₃): δ 8.80 (d, 1 H); 8.54 (m, 1 H); 7.85 (d of t, 1 H); 7.34 (m, 1 H); 7.22 (m, 1 H); 6.94 (d, 1 H); 6.86 (s, 1 H); 6.70 (d of d, 1 H); 3.13 (br, 2 H). MS (API): *m/z* 171 (M + H⁺).

Step 3. (6,7-Diethoxy-quinazolin-4-yl)-(3-pyridin-3-yl-phenyl)amine (3j). A solution of 0.042 g (0.25 mmol) of 3-pyridin-3-yl-phenylamine in 0.80 mL of 2-propanol was heated at reflux and treated with 0.050 g (0.20 mmol) of **7** added in a single portion. The mixture was heated for 2 h, then cooled, and filtered. The precipitate was washed with ethyl acetate and dried to afford 0.068 g (88%) of **3j** as colorless

crystals; mp 255–256 °C. ¹H NMR (DMSO-*d*₆): δ 8.94 (s, 1 H); 8.79 (s, 1 H); 8.61 (d, 1 H); 8.23 (s, 1 H); 8.15 (d, 1 H); 8.06 (s, 1 H); 7.74–7.53 (m, 4 H); 4.23 (overlapping q, 4 H); 1.42 (overlapping t, 6 H). MS (API): *m/z* 387 (M + H⁺). Anal. (C₂₃H₂₂N₄O₂·HCl): C, H, N.

2-[3-(6,7-Diethoxy-quinazolin-4-ylamino)phenyl]thiazole-4-carboxylic Acid Amide (3c). **Step 1. 2-(3-Nitrophenyl)thiazole-4-carboxylic Acid Ethyl Ester (18).** Ethyl bromopyruvate (12 mL, 96 mmol) and 3-nitrothiobenzamide³⁶ (10.93 g, 60 mmol) were heated under reflux in 60 mL of ethanol for 30 min. The mixture was cooled, and the precipitate was washed with ethanol and dried to afford 8.805 g (53%) of **18** as white crystals; mp 142–145 °C. ¹H NMR (CDCl₃): δ 8.84 (m, 1 H); 8.39 (d, 1 H); 8.32 (d, 1 H); 8.27 (s, 1 H); 7.68 (t, 1 H); 4.48 (q, 2 H); 1.46 (t, 3 H). MS (API): *m/z* 279 (M + H⁺). Anal. (C₁₂H₁₀N₂O₄S): C, H, N.

Step 2. 2-(3-Nitrophenyl)thiazole-4-carboxylic Acid Amide (19). A mixture of 8.705 g (31 mmol) of **18** and 31 mL of 4 M potassium hydroxide in 35 mL of tetrahydrofuran (THF) and 35 mL of methanol was heated at reflux for 90 min. The mixture was cooled and concentrated. The residue was dissolved in hot water (800 mL) and filtered and then acidified with 6 M hydrochloric acid while still hot. Filtration and drying afforded 6.33 g (80%) of the acid as white flakes. The acid was suspended in 50 mL of THF, and 0.5 mL of DMF was added followed by 2.31 mL (26.5 mmol) of oxalyl chloride. After gas evolution had ceased, the clear solution was poured into a mixture of 90 mL of water and 30 mL of concentrated NH₄OH with vigorous stirring. After the mixture was stirred for 20 min, the precipitate was filtered, washed with water, and dried to afford 6.122 g (80%) of **19** as a pale yellow powder; mp 239–241 °C. ¹H NMR (DMSO-*d*₆): δ 8.82 (s, 1 H); 8.842 (d, 1 H); 8.36 (s, 1 H); 8.31 (d, 1 H); 8.08 (br, 1 H); 7.79 (t, 1 H); 7.67 (br, 1 H). MS (API): *m/z* 250 (M + H⁺). Anal. (C₁₀H₇N₃O₃S): C, H, N.

Step 3. 2-(3-Aminophenyl)thiazole-4-carboxylic Acid Amide (20). Tin(II) chloride dihydrate (14.89 g, 66 mmol) was dissolved in 20 mL of concentrated hydrochloric acid with heating. Ethanol (60 mL) was added, followed by 4.98 g (20 mmol) of **19** in three portions. The mixture was heated for 25 min and then poured into a cold solution of 66 g of potassium hydroxide in 750 mL of water. The precipitate was filtered, washed with water, and dried to afford 3.00 g (68%) of **20** as a white powder; mp 173–174 °C. ¹H NMR (DMSO-*d*₆): δ = 8.17 (s, 1 H); 7.70 (br, 1 H); 7.59 (br, 1 H); 7.15–7.08 (m, 3 H); 6.66 (d, 1 H); 5.31 (br, 2 H). MS (API): *m/z* 220 (M + H⁺). Anal. (C₁₀H₉N₃OS): C, H, N.

Step 4. 2-[3-(6,7-Diethoxy-quinazolin-4-ylamino)phenyl]thiazole-4-carboxylic Acid Amide (3c). A solution of 55 mg (0.25 mmol) of **20** in 1 mL of ethanol was heated at reflux and treated with 50 mg (0.2 mmol) of **7**. The mixture was heated at reflux for 1 h, and then, the precipitate was filtered, washed with ethanol, and dried to afford 77 mg (88%) of **3c** as white crystals; mp 284–286 °C. ¹H NMR (DMSO-*d*₆): δ 8.86 (s, 1 H); 8.34 (m, 2 H); 8.29 (m, 1 H); 7.97 (d, 1 H); 7.90 (m, 2 H); 7.70 (br, 1 H); 7.64 (t, 1 H); 7.35 (s, 1 H); 4.27 (overlapping q, 4 H); 1.46 (overlapping t, 6 H). MS (API): *m/z* 436 (M + H⁺). Anal. (C₂₂H₂₁N₅O₃S·HCl): C, H, N.

(6,7-Diethoxy-quinazolin-4-yl)-[4-fluoro-3-(2-methyl-thiazol-4-yl)phenyl]amine (4b). **Step 1. 4-(2-Fluoro-5-nitrophenyl)-2-methyl-thiazole (21).** A solution of 1.83 g (10 mmol) of 1-(2-fluoro-5-nitrophenyl)ethanone³⁷ in 25 mL of glacial acetic acid was treated with 10 mL of 48% HBr followed by 10 mL of 1 M Br₂ in acetic acid. The mixture was stirred at room temperature overnight and then was poured into cold water and extracted with diethyl ether. The extract was washed twice with water, twice with 1 M sodium bicarbonate and brine, dried, and concentrated to afford 2.33 g (89%) of 2-bromo-1-(2-fluoro-5-nitrophenyl)ethanone as a colorless oil, which crystallized slowly on standing. ¹H NMR (CDCl₃): δ 8.81 (m, 1 H); 8.46 (m, 1 H); 7.37 (t, 1 H); 4.47 (s, 2 H). MS (EI): *m/z* 261, 263 (Br isotope pattern, M⁺). This was dissolved in 20 mL of ethanol at reflux and treated with 1.07 g (14.2 mmol) of thioacetamide. Heating was continued

for 30 min, and then, the mixture was cooled and the precipitate was filtered, washed with ethanol, and dried to afford 1.82 g (86%) of **21** as colorless crystals; mp 160–162 °C. ¹H NMR (CDCl₃): δ 9.13 (m, 1 H); 8.16 (m, 1 H); 7.70 (s, 1 H); 7.27 (t, 1 H); 2.78 (s, 3 H). MS (API): *m/z* 239 (M + H⁺). Anal. (C₁₀H₇FN₂O₂S): C, H, N.

Step 2. 4-Fluoro-3-(2-methyl-thiazol-4-yl)phenylamine (22). Tin(II) chloride dihydrate (2.22 g, 9.9 mmol) was dissolved in 3 mL of concentrated hydrochloric acid with heating. Ethanol (15 mL) was added, followed by 0.72 g (3 mmol) of **21**. The mixture was heated for 30 min and then poured into a cold solution of 6.5 g of potassium hydroxide in 70 mL of water. The precipitate was filtered, washed with water, and dried to afford 0.58 g (93%) of **22** as a white powder; mp 73–75 °C. ¹H NMR (CDCl₃): δ 7.58 (m, 2 H); 6.92 (m, 1 H); 6.65 (m, 1 H); 2.77 (s, 3 H). MS (API): *m/z* 209 (M + H⁺). Anal. (C₁₀H₉FN₂S): C, H, N.

Step 3. (6,7-Diethoxy-quinazolin-4-yl)-[4-fluoro-3-(2-methyl-thiazol-4-yl)phenyl]amine (4b). A solution of 52 mg (0.25 mmol) of **22** in 0.8 mL of 2-propanol was heated at reflux and treated with 50 mg (0.2 mmol) of **7**. The mixture was heated at reflux for 1 h, and then, the precipitate was filtered, washed with 2-propanol, and dried to afford 69 mg (82%) of **4b** as white crystals; mp 280–281 °C. ¹H NMR (DMSO-*d*₆): δ 8.80 (s, 1 H); 8.30 (m, 1 H); 8.21 (s, 1 H); 7.88 (s, 1 H); 7.75 (m, 1 H); 7.43 (t, 1 H); 7.32 (s, 1 H); 4.25 (overlapping q, 4 H); 2.69 (s, 3 H); 1.42 (overlapping t, 6 H). MS (API): *m/z* 436 (M + H⁺). Anal. (C₂₂H₂₁FN₄O₂S·HCl): C, H, N.

(2-Dimethylaminomethyl-6,7-diethoxy-quinazolin-4-yl)-[3-(2-methyl-thiazol-4-yl)phenyl]amine (5n, Scheme 3). **Step 1. 2-Chloromethyl-6,7-diethoxy-3H-quinazolin-4-one (14).** A solution of 4.51 g (17.8 mmol) of **13** in 75 mL of chloroacetonitrile was saturated with dry hydrogen chloride gas until the precipitate that initially formed had dissolved. The mixture was stirred at 25 °C for 16 h before it was poured into water (200 mL) and concentrated ammonium hydroxide (30 mL). The precipitate was filtered, washed with water, and suspended in ethanol. The solid was filtered, washed with ethanol, and dried to afford 4.21 g (83%) of **14**; mp 263–265 (dec) °C. ¹H NMR (DMSO-*d*₆): δ 7.38 (s, 1 H); 7.10 (s, 1 H); 4.47 (s, 2 H); 4.13 (q, 2 H); 4.09 (q, 2 H); 1.34 (overlapping t, 6 H). MS (API): *m/z* 283, 284 (M + H⁺, Cl isotope pattern). Anal. (C₁₃H₁₅ClN₂O₃): C, H, N.

Step 2. (2-Chloromethyl-6,7-diethoxy-quinazolin-4-yl)-[3-(2-methyl-thiazol-4-yl)phenyl]amine (5g). A mixture of 2.50 g (8.8 mmol) of **14** in 30 mL of phosphorus oxychloride was heated at reflux for 2 h. The mixture was then cooled and added dropwise to a mixture of 2 g of tribasic sodium phosphate and 200 mL of water with stirring. The mixture was maintained at pH 5 by addition of 6 M sodium hydroxide as needed, while the temperature was maintained below 25 °C by addition of ice. When the addition was complete, the mixture was extracted with chloroform. The combined chloroform extracts were washed three times with water and brine, dried, and concentrated to afford 2.56 g (99%) of 4-chloro-2-chloromethyl-6,7-diethoxy-quinazoline; mp 109–112 °C. ¹H NMR (CDCl₃): δ 7.36 (s, 1 H); 7.33 (s, 1 H); 4.78 (s, 2 H); 4.26 (overlapping q, 4 H); 1.56 (overlapping t, 6 H). MS (API): *m/z* 301, 303, 305 (M + H⁺, 2 Cl isotope pattern). This was dissolved in 20 mL of 2-propanol, and 1.85 g (9.7 mmol) of **15** was added. The mixture was heated under reflux for 2 h and then cooled. The precipitate was filtered, washed with 2-propanol, and dried to afford 3.31 g (83%) of **5g**; mp 252–256 °C. ¹H NMR (DMSO-*d*₆): δ 8.28 (s, 1 H); 8.21 (s, 1 H); 7.91 (s, 1 H); 7.83 (d, 1 H); 7.76 (d, 1 H); 7.47 (t, 1 H); 7.33 (s, 1 H); 4.79 (s, 2 H); 4.24 (q, 2 H); 4.19 (q, 2 H); 2.68 (s, 3 H); 1.39 (overlapping t, 6 H). MS (API): *m/z* 455, 457 (M + H⁺, Cl isotope pattern). Anal. (C₂₃H₂₃ClN₄O₂S·HCl): C, H, N.

Step 3. (2-Dimethylaminomethyl-6,7-diethoxy-quinazolin-4-yl)-[3-(2-methyl-thiazol-4-yl)phenyl]amine (5n). A suspension of 0.113 g (0.25 mmol) of **5g** in 5 mL of 1,4-dioxane was saturated with dimethylamine. The mixture was heated at 80 °C in a sealed tube for 6 h. The mixture was cooled and filtered, and the precipitate was washed with ethanol and

dried to afford 0.094 g (81%) of **5n**; mp 170–172 °C. ¹H NMR (DMSO-*d*₆): δ 9.48 (s, 1 H); 8.56 (s, 1 H); m7.94 (d, 1 H); 7.91 (s, 1 H); 7.86 (s, 1 H); 7.59 (d, 1 H); 7.38 (t, 1 H); 7.14 (s, 1 H); 4.19 (overlapping q, 4 H); 3.57 (s, 2 H); 3.30 (s, 3 H); 2.28 (s, 6 H); 1.41 (overlapping t, 6 H). MS (API): *m/z* 464 (M + H⁺). Anal. (C₂₅H₂₉N₅O₂S): C, H, N.

(6-Ethoxy-7-isopropoxy-quinazolin-4-yl)-[3-(2-methylthiazol-4-yl)phenyl]amine (6p). Step 1. 2-Amino-5-ethoxy-4-isopropoxy-benzoic Acid Ethyl Ester (23). 3-Ethoxy-4-hydroxybenzaldehyde ("ethyl vanillin") was converted to 3-ethoxy-4-isopropoxybenzoic acid by alkylation with 2-bromopropane followed by oxidation with potassium permanganate.³⁸ The acid was subjected to Fischer esterification, nitration, and hydrogenation as described for the preparation of **13**; mp 91–93 °C. ¹H NMR (CDCl₃): δ 7.39 (s, 1 H); 6.37 (s, 1 H); 4.56 (m, 1 H); 4.30 (q, 2 H); 3.98 (q, 2 H); 1.37 (m, 12 H). MS (API): *m/z* 268 (M + H⁺). Anal. (C₁₄H₂₁N₃O₄): C, H, N.

Step 2. 6-Ethoxy-7-isopropoxy-3H-quinazolin-4-one (24). A mixture of 4.86 g (19.2 mmol) of **23** and 2.54 g (24 mmol) of formamide acetate in 60 mL of ethanol was heated at reflux for 5 h. The mixture was cooled and filtered. The precipitate was washed with ethanol–diethyl ether (1:1) and diethyl ether and dried to afford 3.75 g (78%) of **24**; mp 204–205 °C. ¹H NMR (DMSO-*d*₆): δ 7.92 (s, 1 H); 7.39 (s, 1 H); 7.08 (s, 1 H); 4.74 (m, 1 H); 4.07 (q, 2 H); 1.33 (t, 3 H); 1.29 (d, 6 H). MS (API): *m/z* 249 (M + H⁺). Anal. (C₁₃H₁₆N₂O₃): C, H, N.

Step 3. (6-Ethoxy-7-isopropoxy-quinazolin-4-yl)-[3-(2-methylthiazol-4-yl)phenyl]amine (6p). A solution of 0.744 g (3 mmol) of **24** and 0.150 g (1.1 mmol) of triethylamine hydrochloride in 3 mL of phosphorus oxychloride was heated at 120 °C for 3 h. The mixture was concentrated, and the residue was treated with ethyl acetate and 1 M tribasic sodium phosphate and stirred for 30 min. The ethyl acetate was separated, and the washing was repeated. The ethyl acetate was then washed with brine, dried, and concentrated to afford 0.697 g (87%) of 4-chloro-6-ethoxy-7-isopropoxy-quinazoline; mp 104–106 °C. ¹H NMR (CDCl₃): δ 8.81 (s, 1 H); 7.35 (s, 1 H); 7.29 (s, 1 H); 4.77 (m, 1 H); 4.23 (q, 2 H); 1.54 (t, 3 H); 1.47 (d, 6 H). MS (API): *m/z* 267, 269 (M + H⁺, Cl isotope pattern). A solution of 0.067 g (0.25 mmol) of this in 1 mL of ethanol was heated under reflux and treated with 0.057 g (0.30 mmol) of **15**. The mixture was heated for 1 h and then cooled and allowed to stand at 20 °C for 16 h. The precipitate was filtered, washed with ethanol, and dried to afford 0.093 g (88%) of **6p**; mp 257–259 °C. ¹H NMR (DMSO-*d*₆): δ 8.79 (s, 1 H); 8.16 (m, 2 H); 7.97 (s, 1 H); 7.83 (d, 1 H); 7.68 (d, 1 H); 7.50 (t, 1 H); 7.36 (s, 1 H); 4.77 (m, 1 H); 4.25 (q, 2 H); 2.69 (s, 3 H); 1.42 (t, 3 H); 1.37 (d, 6 H). MS (API): *m/z* 421 (M + H⁺). Anal. (C₂₃H₂₄N₄O₂S HCl): C, H, N.

Fructose-1,6-bisphosphatase Enzyme Assay. Fructose-1,6-bisphosphatase (F16BP) was assayed by measuring its ability to hydrolyze inorganic phosphate from fructose-1,6-bisphosphate using a modification of a reported method.³⁹ Specifically, 20 μL of rabbit, rat, human, or porcine F16BPase (20–60 ng depending on species⁴⁰) was added to 80 μL of substrate and compound in a 96 well microtiter plate to start the reaction. The final solution consisted of 50 mM HEPES, pH 7.2, 100 mM KCl, 2 mM MgCl₂, 2 mM EGTA, 1 mM DTT, and 500 μM fructose-1,6-bisphosphate. The solution was incubated for 40 min at room temperature without preincubation of compound with enzyme. The phosphate released by the enzyme was measured spectrophotometrically using a Titertek Multiscann MCC 340 at 620 nm, after the phosphate was allowed to form a complex for 10 min after the addition of 150 μL of ammonium molybdate/malachite green (AM/MG) solution. To prepare the AM/MG solution, one volume of 4.2% ammonium molybdate (w/v) in 4 M hydrochloric acid was added to three volumes of 0.045% malachite green (w/v) and 0.01% Tween-20 (v/v) in water. The AM/MG solution was stirred at room temperature for 30 min and filtered through a 0.22 μm filter before it was added to each reaction well. The assay was run under saturating concentrations of substrate due to the low *K_m* of F16BPase for its substrate and the relatively low sensitivity of the phosphate detection method.

Under these conditions, the assay was linear with time and enzyme concentration, and it was able to detect allosteric inhibitors of F16BP (IC₅₀ of AMP against the human enzyme = 0.8 μM).

Site-Directed Mutagenesis of Rat F16BPase. Mutagenesis of the rat F16BPase cDNA in expression plasmid pET 23b was carried out using the QuikChange mutagenesis kit from Stratagene (La Jolla, Ca). The Gln50Lys mutation was generated with an oligonucleotide primer of the following sequence: 5'-CGCAAGGCCGGCATCGCTCAG CTC-3'. The sequence of the primer for the Gln55His mutation was 5'-CGCCAGGCCGGCATCGCTCACTC-3'. The double mutant primer (Gln50Lys,Gln55His) sequence was 5'-CGCAAGGCCGGCATCGCTCACTC-3'. Nucleotide changes resulting in the codon alterations are highlighted in boldface and italicized. The sequences described above encode the sense strand; both the sense strand primers and their complements were used to generate the mutated plasmids. Sequence confirmation was carried out on all resultant plasmids to ensure their fidelity. Wild-type recombinant enzyme and the respective mutant derivatives were expressed in *E. coli* strain BL21(DE3) and purified as described previously.⁴²

Enzyme Crystallization. Recombinant porcine kidney F16BPase was concentrated in 8 mM pH 7.2 potassium phosphate buffer containing 1 mM EDTA, 1 mM β-mercaptoethanol, 0.5 mM manganous chloride, and 1 mM **25** to a protein concentration of 15 mg mL⁻¹. AMP and fructose-6-phosphate were added to obtain a final concentration of 1 mM each and then incubated for 60 min at room temperature prior to crystallization trials using the hanging drop vapor diffusion method. The drops consisted of 2 μL of protein mixed with 2 μL of 100 mM pH 7.0 HEPES containing 200 mM sodium acetate and 13.5% PEG 4000 and suspended over 600 μL of the same buffer. T state crystals grew within 1 week and reached a maximum size of 0.4 mm × 0.04 mm × 0.3 mm. Crystals were then soaked in 2 mM **2g** or other potent inhibitors of interest and were used for data collection. The inhibitors were added to the crystals in the crystallization drop from a dilution of a 250 mM stock solution in DMSO such that the final DMSO concentration was <1%.

Data Collection and Structure Determination. The crystal was subjected to cryostabilization conditions by quick immersion into crystallization buffer with 10% MPD and then frozen at 100 K. Diffraction data were collected on a Rigaku Raxis II image plate detector using a Rigaku RU-200 generator equipped with Molecular Structure Corporation focusing mirrors. There were 54 052 unique reflections in the data set with a resolution limit of 2 Å, 93.9% completeness in the highest resolution shell with an overall completeness of 97.9%, and *R_{merge}* of 0.044.

The space group of these crystals was found to be *P2₁2₁2₁*, with unit cell dimensions *a* = 59.65 Å *b* = 165.94 Å, and *c* = 79.22 Å with two monomers of F16BPase in the crystallographic asymmetric unit. This is isomorphous with the space group and unit cell dimensions of previously published T state structures of F16BPase (pdb references: 1FBP, 1FPD),⁴¹ so a starting model for rigid body refinement was derived from the protein coordinates in pdb entry 1FPD. Examination of difference Fourier maps, after rigid body and individual atom positional refinement of the protein atoms, showed clear density for AMP and F6P at the allosteric and substrate binding sites, respectively. Two manganese ions could also be placed in the electron density. In addition, some unexplained electron density was seen at the tetramer interface, but it could not be unambiguously fit to the inhibitor. We then soaked these crystals into a solution containing 2mM **2g** for 1 week. Difference Fourier maps calculated after refinement of the protein model again showed clear electron density for AMP, F6P, and two manganese ions. In addition, clear electron density could be seen at the subunit interface, into which two molecules of **2g** could be readily modeled. The structure was refined using REFMAC from the CCP4 suite of programs to a final *R*-factor of 0.188 and free *R*-factor of 0.238.

Acknowledgment. We thank Professor Evan R. Kantrowitz (Boston College) for a supply of porcine kidney F16BPase. We thank Professor M. Raafat El-Maghrabi (SUNY Stony Brook) for the kind provision of the human and rat F16BPase cDNAs. We also thank Dr. James D. Moyer for collaboration with the EGFR tyrosine kinase inhibition assay and Dr. Rodney C. Schnur for the preparation of **2a**.

Supporting Information Available: IC₅₀ values for compounds **2–6** vs recombinant human liver F16BPase, purified native rabbit liver F16BPase, recombinant rat liver F16BPase, and recombinant porcine kidney F16BPase. This material is available free of charge via the Internet at <http://pubs.acs.org>.

References

- (1) (a) Kolterman, O. G.; Gray, R. S.; Griffin, J.; Burstein, P.; Insel, J.; Scarlett, J. A.; Olefsky, J. M. Receptor and Postreceptor Defects Contribute to the Insulin Resistance in Noninsulin-dependent Diabetes Mellitus. *J. Clin. Invest.* **1981**, *68*, 957–969. (b) DeFronzo, R. A. The Triumvirate: Beta Cell, Muscle, Liver. A Collusion Responsible for NIDDM. *Diabetes* **1988**, *37*, 667–687.
- (2) (a) Rothman, D. L.; Magnusson, I.; Katz, L. D.; Shulman, R. G.; Shulman, G. I. Quantitation of Hepatic Glycogenolysis and Gluconeogenesis in Fasting Humans with ¹³C NMR. *Science* **1991**, *254*, 573–576. (b) Magnusson, I.; Rothman, D. L.; Katz, L. D.; Shulman, R. G.; Shulman, G. I. Increased Rate of Gluconeogenesis in Type II Diabetes Mellitus. A ¹³C Nuclear Magnetic Resonance Study. *J. Clin. Invest.* **1992**, *90*, 1323–1327. (c) Consoli, A.; Nurjhan, N.; Capani, F.; Gerich, J. Predominant Role of Gluconeogenesis in Increased Hepatic Glucose Production in NIDDM. *Diabetes* **1989**, *38*, 550–557. (d) Giaccari, A.; Morviducci, L.; Pastore, L.; Zorretta, D.; Sbraccia, P.; Maroccia, E.; Buongiorno, A.; Tamburrano, G. Relative Contribution of Glycogenolysis and Gluconeogenesis to Hepatic Glucose Production in Control and Diabetic Rats. A Reexamination in the Presence of Euglycaemia. *Diabetologia* **1998**, *41*, 307–314.
- (3) Pilkis, S. J.; Granner, D. K. Molecular physiology of the regulation of hepatic gluconeogenesis and glycolysis. *Annu. Rev. Physiol.* **1992**, *54*, 885–909.
- (4) (a) Insulin resistant model: Sugiyama, Y.; Shimura, Y.; Ikeda, H. Pathogenesis of Hyperglycemia in Genetically Obese-Hyperglycemic Rats, Wistar Fatty: Presence of Hepatic Insulin Resistance. *Endocrinol. Jpn.* **1989**, *36*, 65–73. (b) Insulin deficient model: Wilmhurst, J. M.; Manchester, K. L. A Comparison of the Effects of Diabetes Induced with either Alloxan or Streptozotocin and of Starvation on the Activities in Rat Liver of the Key Enzymes of Gluconeogenesis. *Biochem. J.* **1970**, *120*, 95–103.
- (5) (a) For a review, see Veneziale, C. M.; Donofrio, J. C.; Hansen, J. B.; Johnson, M. L.; Mazzotta, M. Y. Intracellular Concentration and Specific Activity of Carbohydrate – Metabolizing Enzymes. Application of Specific Radioimmunoassays. In *The Regulation of Carbohydrate Formation and Utilization in Mammals*; Veneziale, C. M., Ed.; University Park Press: Baltimore, 1981; pp 23–44. (b) Pilkis, S. J.; Granner, D. K. Molecular Physiology of the Regulation of Hepatic Gluconeogenesis and Glycolysis. *Annu. Rev. Physiol.* **1992**, *54*, 885–909.
- (6) (a) Van Schaftingen, E.; Hers, H.-G. Inhibition of Fructose-1,6-bisphosphatase by Fructose 2,6-Bisphosphate. *Proc. Natl. Acad. Sci. U.S.A.* **1981**, *78*, 2861–2863. (b) Pilkis, S. J.; El-Maghrabi, M. R.; Pilkis, J.; Claus, T. Inhibition of Fructose-1,6-bisphosphatase by Fructose 2,6-Bisphosphate. *J. Biol. Chem.* **1981**, *256*, 3619–3622. (c) Pilkis, S. J.; El-Maghrabi, M. R.; Claus, T. H. Hormonal Regulation of Hepatic Gluconeogenesis and Glycolysis. *Annu. Rev. Biochem.* **1988**, *57*, 755–783.
- (7) (a) Taketa, K.; Pogell, B. M. Allosteric Inhibition of Rat Liver Fructose 1,6-Diphosphatase by Adenosine 5'-Monophosphate. *J. Biol. Chem.* **1965**, *240*, 651–662. (b) Ke, H.; Liang, J.-Y.; Zhang, Y.; Lipscomb, W. N. Conformational Transition of Fructose-1,6-bisphosphatase: Structure Comparison between the AMP Complex (T form) and the Fructose 6-Phosphate Complex (R form). *Biochemistry* **1991**, *30*, 4412–4420. (c) Zhang, Y.; Liang, J.-Y.; Huang, S.; Lipscomb, W. N. Toward a Mechanism for the Allosteric Transition of Pig Kidney Fructose-1,6-Bisphosphatase. *J. Mol. Biol.* **1994**, *244*, 609–624.
- (8) Gidh-Jain, M.; Zhang, Y.; van Poelje, P. D.; Liang, J.-Y.; Huang, S.; Kim, J.; Elliott, J. T.; Erion, M. D.; Pilkis, S. J.; El-Maghrabi, M. R.; Lipscomb, W. N. The Allosteric Site of Human Liver Fructose-1,6-Bisphosphatase. *J. Biol. Chem.* **1994**, *269*, 27732–27738.
- (9) Gruber, H. E.; Tuttle, R. E.; Browne, C. E.; Ugarkar, B. G.; Reich, J. W.; Metzner, E. K.; Marangos, P. J. Preparation of produg forms of 1-β-D-ribofuranosyl-5-aminoimidazole-4-carboxamide, and their use in lowering blood glucose and treatment of blood-glucose-related disorders. WO 90/09163 A2, 1990; *Chem. Abstr.* **1991**, *114*, 214418.
- (10) (a) Dang, Q.; Erion, M. D.; Reddy, M. R.; Scarlato, G. R.; Kasibhatla, S. R.; Reddy, K. R. Preparation of benzimidazolylphosphonates as inhibitors of fructose-1,6-bisphosphatase. WO 98/39343 A1, 1998; *Chem. Abstr.* **1998**, *129*, 245147. (b) Dang, Q.; Erion, M. D.; Reddy, M. R.; Robinson, E. D.; Kasibhatla, S. R.; Reddy, K. R. Preparation of novel purines for use as inhibitors of fructose-1,6-bisphosphatase. WO 98/39344 A1, 1998; *Chem. Abstr.* **1998**, *129*, 260281. (c) Dang, Q.; Erion, M. D.; Reddy, M. R.; Scarlato, G. R.; Kasibhatla, S. R.; Reddy, K. R. Preparation of indoles and aza-indoles as inhibitors of fructose-1,6-bisphosphatase. WO 98/39342 A1, 1998; *Chem. Abstr.* **1998**, *129*, 245033. (d) Dang, Q.; Kasibhatla, S. R.; Reddy, K. R.; Erion, M. D.; Reddy, M. R.; Agarwal, A. Preparation of heteroaromatic phosphonates as fructose 1,6-bisphosphatase inhibitors. WO 00/14095 A1, 2000; *Chem. Abstr.* **2000**, *132*, 222529.
- (11) Mjalli, A. M. M.; Mason, J. C.; Arienti, K. L.; Short, K. M.; Kimmich, R. D. A.; Jones, T. K. Preparation of dioxopiperazinoacetamides as fructose-1,6-bisphosphatase inhibitors. WO 99/47549 A1, 1999; *Chem. Abstr.* **1999**, *131*, 243287.
- (12) Wright, S. W.; Hageman, D. L.; McClure, L. D.; Carlo, A. A.; Treadway, J. L.; Mathiowetz, A. M.; Withka, J. M.; Bauer, P. H. Allosteric Inhibition of Fructose-1,6-Bisphosphatase by Anilinoquinazolines. *Bioorg. Med. Chem. Lett.* **2001**, *11*, 17–21.
- (13) El-Maghrabi, M. R.; Gidh-Jain, M.; Austin, L. R.; Pilkis, S. J. Isolation of a Human Liver Fructose-1,6-bisphosphatase cDNA and Expression of the Protein in *Escherichia coli*. *J. Biol. Chem.* **1993**, *268*, 9466–9472.
- (14) Baykov, A. A.; Evtushenko, O. A.; Awaeva, S. M. A Malachite Green Procedure for Orthophosphate Determination and Its Use in Alkaline Phosphatase-Based Enzyme Immunoassay. *Anal. Biochem.* **1988**, *171*, 266–270.
- (15) El-Maghrabi, M. R.; Pilkis, J.; Marker, A. J.; Colosia, A. D.; D'Angelo, G.; Fraser, B. A.; Pilkis, S. J. cDNA Sequence of Rat Liver Fructose-1,6-bisphosphatase and Evidence for Down-regulation of its mRNA by Insulin. *Proc. Natl. Acad. Sci. U.S.A.* **1988**, *85*, 8430–8434.
- (16) Giroux, E.; Williams, M. K.; Kantrowitz, E. R. Shared Active Sites of Fructose-1,6-bisphosphatase. *J. Biol. Chem.* **1994**, *269*, 31404–31409.
- (17) Commercially available (Sigma) rabbit liver F16BPase (<10% pure) was purified to 95+% purity; see (a) Pontremoli, S.; Traniello, S.; Luppis, B.; Wood, W. A. Fructose Diphosphatase from Rabbit Liver. *J. Biol. Chem.* **1965**, *240*, 3459–3463. (b) Pontremoli, S.; Grazi, E.; Accorsi, A. Fructose Diphosphatase from Rabbit Liver. X. Isolation and Kinetic Properties of the Enzyme-Adenosine Monophosphate Complex. *Biochemistry* **1968**, *7*, 3628–3633.
- (18) Fry, D. W.; Kraker, A. J.; McMichael, A.; Ambrosio, L. A.; Nelson, J. M.; Leopold, W. R.; Connors, R. W.; Bridges, A. J. A Specific Inhibitor of the Epidermal Growth Factor Receptor Tyrosine Kinase. *Science* **1994**, *265*, 1093–1095.
- (19) Similar attempts to discern the mode of binding of **1** by NMR spectroscopy or X-ray crystallography were confounded by the insolubility of this compound; see ref 11.
- (20) For example, analogues of **2a** in which the 6,7-diethoxy substitution pattern was replaced by 6-Cl, 6-NO₂, 6-AcNH, 6-PhO, 7-CO₂Me, 7-CO₂H, 7-CONEt₂, 7-NO₂, 7-NH₂, or 7-AcNH were all inactive against human F16BPase (unpublished results).
- (21) (a) Kurbanov, F. T.; Choe, J.-Y.; Honzatko, R. B.; Fromm, H. J. Directed Mutations in the Poorly Defined Region of Porcine Liver Fructose-1,6-bisphosphatase Significantly Affect Catalysis and the Mechanism of AMP Inhibition. *J. Biol. Chem.* **1998**, *273*, 17511–17516. (b) Choe, J.-Y.; Poland, B. W.; Fromm, H. J.; Honzatko, R. B. Role of a Dynamic Loop in Cation Activation and Allosteric Regulation of Recombinant Porcine Fructose-1,6-bisphosphatase. *Biochemistry* **1998**, *37*, 11441–11450. (c) Nelson, S. W.; Iancu, C. V.; Choe, J.-Y.; Honzatko, R. B.; Fromm, H. J. Tryptophan Fluorescence Reveals the Conformational State of a Dynamic Loop in Recombinant Porcine Fructose-1,6-bisphosphatase. *Biochemistry* **2000**, *39*, 11100–11106.
- (22) Nelson, S. W.; Choe, J.-Y.; Honzatko, R. B.; Fromm, H. J. Mutations in the Hinge of a Dynamic Loop Broadly Influence Functional Properties of Fructose-1,6-bisphosphatase. *J. Biol. Chem.* **2000**, *275*, 29986–29992.
- (23) Carcamo, J. G.; Yanez, A. J.; Ludwig, H. C.; Leon, O.; Pinto, R. O.; Reyes, A. M.; Slebe, J. C. The C1–C2 Interface Residue Lysine 50 of Pig Kidney Fructose-1,6-bisphosphatase Has a Crucial Role in the Cooperative Signal Transmission of the AMP Inhibition. *Eur. J. Biochem.* **2000**, *267*, 2242–2251.

- (24) (a) Ke, H.; Zhang, Y.; Lipscomb, W. N. Crystal Structure of Fructose-1,6-bisphosphatase Complexed with Fructose 6-Phosphate, AMP, and Magnesium. *Proc. Natl. Acad. Sci. U.S.A.* **1990**, *87*, 5243–5247. (b) Shyur, L.-F.; Aleshin, A. E.; Honzatko, R. B.; Fromm, H. J. Biochemical Properties of Mutant and Wild-type Fructose-1,6-bisphosphatases are Consistent with the Coupling of Intra- and Intersubunit Conformational Changes in the T- and R-state Transition. *J. Biol. Chem.* **1996**, *271*, 33301–33307.
- (25) (a) Jencks, W. P. On the Attribution and Additivity of Binding Energies. *Proc. Natl. Acad. Sci. U.S.A.* **1981**, *78*, 4046–4050. (b) This approach has been used with glycogen phosphorylase, for example, see Rath, V. L.; Ammirati, M.; Danley, D. E.; Ekstrom, J. L.; Gibbs, E. M.; Hynes, T. R.; Mathiowetz, A. M.; McPherson, R. K.; Olson, T. V.; Treadway, J. L.; Hoover, D. J. Human Liver Glycogen Phosphorylase Inhibitors Bind at a New Allosteric Site. *Chem. Biol.* **2000**, *7*, 677–682.
- (26) Lipinski, C. A. Drug-Like Properties and the Causes of Poor Solubility and Poor Permeability. *J. Pharmacol. Toxicol. Methods* **2001**, *44*, 235–249.
- (27) Structures **18** and **19** are shown only to illustrate the concept presented. They are not optimized structures, and computational evaluation of them indicates that they would not dock properly at this binding site. It should be recognized that a second-generation inhibitor identified by computational chemistry that binds unimolecularly at this site may look nothing like the anilinoquinazolines lead structures.
- (28) (a) Gidh-Jain, M.; Zhang, Y.; van Poelje, P. D.; Liang, J.-Y.; Huang, S.; Kim, J.; Elliott, J. T.; Erion, M. D.; Pilakis, S. J.; El-Maghrabi, M. R.; Lipscomb, W. N. The Allosteric Site of Human Liver Fructose-1,6-bisphosphatase. *J. Biol. Chem.* **1994**, *269*, 27732–27738. (b) Iversen, L. F.; Brzozowski, M.; Hastrup, S.; Hubbard, R.; Kastrup, J. S.; Larsen, I. K.; Naerum, L.; Nørskov-Lauridsen, L.; Rasmussen, P. B.; Thim, L.; Wiberg, F. C.; Lundgren, K. Characterization of the Allosteric Binding Pocket of Human Liver Fructose-1,6-bisphosphatase by Protein Crystallography and Inhibitor Activity Studies. *Protein Sci.* **1997**, *6*, 971–982.
- (29) See refs 12 and 14.
- (30) This compound was prepared from commercially available 3,4-diethoxybenzoic acid by Fischer esterification with ethanol using concentrated sulfuric acid as a catalyst; mp 56–57 °C.
- (31) Hudson, A. T.; Vile, S.; Barraclough, P.; Franzmann, K. W.; McKeown, S. C.; Page, M. J. Preparation of Quinoline and Quinazoline Protein Tyrosine Kinase Inhibitors. WO 96/09294 A1, 1996; *Chem. Abstr.* **1996**, *125*, 114665.
- (32) Behera, G. B.; Kar, J. N.; Acharya, R. C.; Rout, M. K. Quaternization of Thiazoles. *J. Org. Chem.* **1973**, *38*, 2164–2166.
- (33) Zhang, M. Q.; Haemers, A.; Vanden Berghe, D.; Pattyn, S. R.; Bollaert, W.; Levshin, I. Quinolone antibacterials. 1. 7-(2-Substituted-4-thiazolyl- and -Thiazolidinyl)quinolones. *J. Heterocycl. Chem.* **1991**, *28*, 673–683.
- (34) (a) Leclerc, G.; Marciniak, G.; Decker, N.; Schwartz, J. Cardiotonic Agents. 2. Synthesis and Structure–Activity Relationships in a New Class of 6-, 7-, and 8-Pyridyl-2(1H)-quinolone Derivatives. *J. Med. Chem.* **1986**, *29*, 2433–2438. (b) Haworth, J. W.; Heilbron, I. M.; Hey, D. H. Arylpyridines. Part 1. Phenylpyridines and Nitrophenylpyridines. *J. Chem. Soc.* **1940**, 349–355.
- (35) Heilbron, I. M.; Hey, D. H.; Lambert, A. Arylpyridines. Part 4. 3- and 4-Pyridyldiphenyls. *J. Chem. Soc.* **1940**, 1279–1284.
- (36) Taylor, E. C.; Zoltewicz, J. A. A New Synthesis of Aliphatic and Aromatic Thioamides from Nitriles. *J. Am. Chem. Soc.* **1960**, *82*, 2656–2657.
- (37) Cooper, C. S.; Klock, P. L.; Chu, D. T. W.; Fernandes, P. B. The Synthesis and Antibacterial Activities of Quinolones Containing Five- and Six-Membered Heterocyclic Substituents at the 7-Position. *J. Med. Chem.* **1990**, *33*, 1246–1252.
- (38) 3-Ethoxy-4-isopropoxybenzoic acid was prepared from 3-ethoxy-4-hydroxybenzaldehyde (“ethyl vanillin”) by alkylation with 2-bromopropane and subsequent oxidation with potassium permanganate; see Kirk, T. K.; Lorenz, F. L. Oxygenation of 4-Alkoxy Groups in Alkoxybenzoic Acids by *Polyporus dichrous*. *Appl. Microbiol.* **1974**, *27*, 360–367.
- (39) Harder, K. W.; Owen, P.; Wong, L. K. H.; Aebersold, R.; Clarke-Lewis, I.; Jirik, F. R. Characterization and Kinetic Analysis of the Intracellular Domain of Human Protein Tyrosine Phosphatase Beta Using Synthetic Phosphopeptides. *Biochem. J.* **1994**, *298*, 395–401.
- (40) Assays were conducted with the following amounts of F16BPase enzymes: human, 60 ng/well; rabbit, 22 ng/well; rat, 40 ng/well; porcine, 20 ng/well.
- (41) See ref 22a.
- (42) El-Maghrabi, M. R.; Pilakis, S. J. Expression of Rat Liver Fructose-1,6-Bisphosphatase in *Escherichia Coli*. *Biochem. Biophys. Res. Commun.* **1991**, *176*, 137–144.

JM010496A